九州大学学術情報リポジトリ
Kyushu University Institutional Repository

Studies on Sn Thin Film Decomposition Using VHF Hydrogen Plasmas

吉, 梦然

https://hdl.handle.net/2324/4475167

出版情報：Kyushu University, 2020, 博士（工学）, 課程博士
バージョン：
権利関係：

Studies on Sn Thin Film Decomposition Using VHF Hydrogen Plasmas

MENGRAN JI

Department of Applied Science for Electronics and Materials

Interdisciplinary Graduate School of Engineering Sciences

Kyushu University

February, 2021

Contents

Chapter1 General Introduction 1

1.1 Introduction 1

1.2 Aim of this study 6

1.3 Outline of this thesis 6

References 8

Chapter 2 VHF Plasma Decomposition and Analysis Methods 11

2.1 Overview 11

2.2 Principle of VHF plasma and diagnostic technique 12

2.2.1 VHF plasma 12

2.2.2 Langmuir probe method 15

2.3 Principle of Sn decomposition 20

2.4 Analysis methods 24

References 29

Chapter 3 Investigation of Basic Characteristics of Sn Thin Film Decomposition 30

3.1 Introduction 30

3.2 Experimental Setup 31

3.3 Results and discussion 35

3.4 Conclusion 45

References 46

Chapter 4 Effect of Hydrogen Ion Energy in the Process of Reactive Ion Etching of Sn Thin Films by Hydrogen Plasmas 48

4.1 Introduction 48

4.2 Experimental setup and methods..49

4.3 Experimental results and discussion..54

4.4 Conclusion..61

References 62

Chapter 5 Conclusion 63

5.1 Summary of this study..63

5.2 Suggestion for the future work...64

Acknowledgement..66

Chapter1 General Introduction

1.1 Introduction

Nowadays, semiconductors and the manufacturing have become indispensable in almost all fields, especially in storage and communication technologies. Much tinier integrated fabrication is required. Based on Moore's Law [1], the performance of semiconductors has been densified at an astonishing rate of doubling in 18 to 24 months, ensuring to support the dramatic progress of semiconductor devices. Further developments of semiconductor devices are still required in various fields. Moreover, further mass of semiconductor integrated circuits is required. Lithography technology is a particularly important technology for realizing the high-volume manufacturing of semiconductor integrated circuits. The progress in semiconductor integration as described above has been supported by the remarkable development in lithography technology. Figure 1.1 shows the advance in wavelength of lithography with years. To the early manufacturing of deep ultraviolet lithography (DUV) has been developed to decrease minimum size of semiconductors. Since 1990s, KrF excimer laser employed wavelength of 248nm [2]. In 2000s, ArF excimer laser with a wavelength of 193nm has been adopted [3]. However, DUV lithography has reached its resolution limitation wavelength minimization of light source, which is difficult to satisfy the ideal situation for a long time.

Extreme ultraviolet light (EUV light) with a wavelength of 13.5 nm has been expected as the light source [4-7]. Although this EUV lithography technology using EUV light was put into practical use in 2018, in fact the realization of practical EUV lithography devices has been delayed by more than 10 years from the original schedule. In order to optimize the high potential of EUV lithography, further research and development are still needed.

Although EUV lithography is an ideal light source, one of the urgent issues of EUV lithography is the insufficient output of light source. Semiconductor processing capacity depends on the line width of

circuits, meaning narrower lines and more capable chips. The utilization of EUV enables the width of line less than 7 nm with 1nm equal to one billionth of a meter. Thus, four times the number of transistors can fit on a semiconductor with a width of 5 nm than on one of 10 nm [8,9]. EUV exposure equipment is indispensable in fitting a 5 nm circuit on a silicon wafer. Within the wavelength range of EUV light, the light absorption of substances is strong, and in conventional devices, air and optical lenses absorb EUV light. Therefore, in the EUV exposure apparatus, it is necessary to maintain all the optical paths in a vacuum and use a reflective lens instead of a transparent lens. Thus, in order to reflect EUV light with an appropriate reflectance, a technique using reflection of a condenser mirrors has been established. By using reflection via condenser mirrors, it is possible to reflect EUV light with a wavelength of 13.5 nm at a peak value of approximately 70 [10]. Although, the current EUV exposure system uses 11 lenses, so the light on the exposed surface is only about 1.4% of the original light. Therefore, in order to realize practical throughput, it is required that the output of the light source achieves over 250W [11-13].

EUV photons are created by the high-density laser produced Sn plasma [14,15]. It uses radiation from Sn multivalent ions to obtain light with a wavelength of 13.5 nm, finally high-density plasmas are generated. Moreover, when EUV photons (with photon energy of 92eV) are absorbed by hydrogen molecules which are filled in the chamber of the EUV generation system, photoelectrons with a kinetic energy of approximately 78-86 eV [16,17] are created. The tin droplet with a size of more than 20 μm is irradiated with a CO_2 laser to generate a high-temperature high-density Sn plasmas. EUV light output at several hundreds of watts is proved to be realized. During this process, the condenser mirrors are directly exposed to the EUV plasma, then Sn debris adhere on the mirrors leading to reflectivity deterioration. The deterioration of reflectance includes three main ways: sputtering, implantation and deposition. The first two damages are irreversible and are caused by high energy (over 10keV) particles. Reflection decreasing due to Sn adhesion can be viewed from the perspective of the expected lifetime of the optical element. EUV lithography requires a lifetime of at least 3×10^4 hours for projection condenser mirrors [18,19]. Meanwhile, collector optics are exchangeable and only expected to hold for 3000 hours.

Because damage caused by deposition is reversible, a proper cleaning measure can be applied to deal with this issue. The most common measure to remove Sn deposition from mirror is employing hydrogen radicals to etch Sn by forming the volatile gas SnH_4 [20-22]. It is known that Sn deposition can be etched by atomic hydrogen, which chemically react with Sn to form SnH_4. The group of D. Ugur [23,24] investigated the decomposition of tin through a chemical reaction using a hydrogen atom flux generated by dissociating hydrogen molecules with a hot filament. As a result, it was reported that one tin atom was removed for every 100,000 hydrogen atoms. The low etching rate is supposed that the readhesion of Sn was taken place on the surface. When this measure is applied to a real EUV system, the problem is how to deliver hydrogen radicals in front of the condenser mirror. In our previous experiments, Sn readhesion was obviously observed on the surface of Sn coated samples, even though the density of hydrogen radicals increased through increasing gas pressure. It is supposed that mean free path of SnH_4 in the hydrogen gas is important for the Sn readhesion process. According to Tamaru [25], the dissociation rate coefficient of SnH_4 increases by one order when gas temperature increases 60℃. Therefore, the production of high density plasmas (high density hydrogen atoms) and the control of gas temperature are the key issues to promote Sn etching process. Also, hydrogen gas flow control is also important for the SnH_4 decomposition.

Moreover, in our previous experiment, hollow cathode discharge was observed in a hole of the earth electrode. It is well known that the hollow-cathode discharge can produce a high density plasma with a simple structure of the hollow electrode [26,27]. The hollow-cathode effect was recognized in 1916 by Paschen [28]. Hollow cathodes are very useful electron generating devices. When gas pressure is low hollow-cathode discharge happens in the cathode hollow cylinder, electrons are trapped in the hollow cylinder while diameter of cylinder is bigger than thickness of ion sheath. Thus, to generate hollow-cathode discharge the re-design of experimental setup has been done in this study, which will be introduced in chapter 3.

On the other hand, reactive ion etching applied on Sn decomposition is proved to be effective [29-31]. RIE (Reactive ion retching) is a well-known phenomenon which is widely employed in surface

process and semiconductor manufacturing, especially applied to pattern transfer dry etching and primary silicon technology. RIE can raise etch rate because incident ions break bonds between surface molecules. The process of Sn decomposition by hydrogen plasmas becomes more efficient, when hydrogen ions provide sufficient energies to break Sn-Sn bonds of Sn films. The team of Illinois university showed by their experiments (which will be described precisely in Chapter 4) that the Sn etch rate was significantly enhanced when bias voltage of about -300 V was added to the Sn-coated samples. The 300 W RF power source was applied to a reactor with 300 mm of diameter. The experiment was performed at a gas pressure of 65 mTorr and a gas flow rate of 100 sccm. The peak etching rate of their study is 1.7nm/min, and approximately 30 hydrogen ions remove one Sn atom. This result shows that hydrogen ions combined with hydrogen atoms are two thousand times efficient for Sn decomposition than hydrogen atoms alone. The problem of their study is that they only investigated the dependence of etching rate on RF power. They did not recognize the importance of parameters such as gas pressure and gas flow rate, and also concluded that the Sn readhesion on surfaces could be ignored. Other proceeding studies [23,24,30,31] have proved one of the main problems to clean EUV optics is the readhesion of Sn.

Based on backgrounds described above, the basic parameters need to be investigated for the Sn decomposition in this study are gas pressure, gas flow rate and gas or material surface temperatures. Furthermore, the role of the hydrogen ion energy in the process of reactive ion etching of Sn.

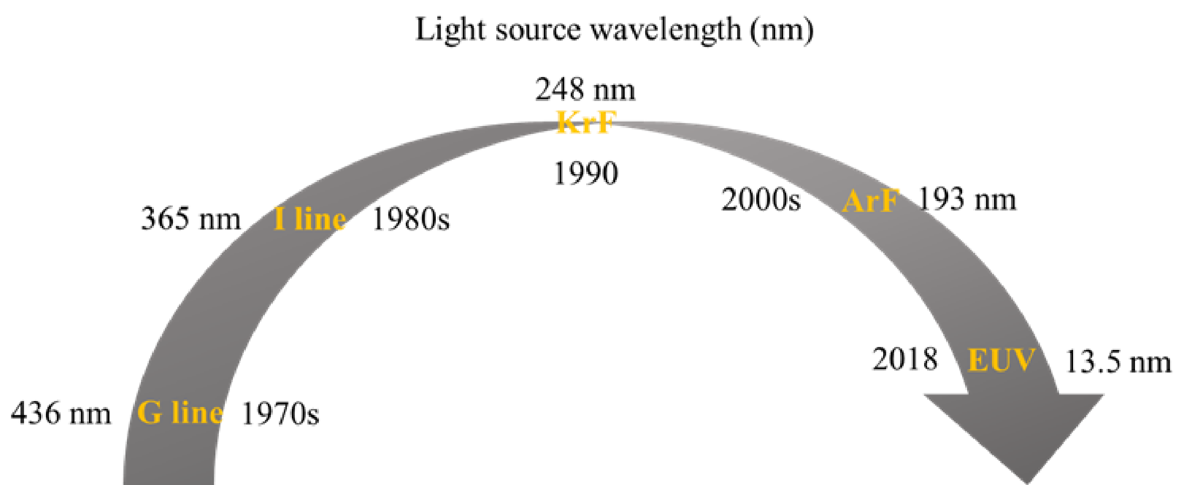

Fig. 1.1 Advance in wavelength of lithography technology.

1.2 Aim of this study

The aim of this study is to clarify the mechanism of Sn decomposition by hydrogen plasmas. This makes it possible to present conditions for efficiently removing the tin film deposited on the mirrors of an actual EUV light source system. Furthermore, we also try to develop a plasma device as an additional tin remover. In this study, a VHF (very high-frequency; 60MHz) power source was proposed to use for the plasma production because it has many advantages over the conventional RF (ratio-frequency) source [32]. VHF plasmas have higher electron density and lower electron temperature compared to the RF plasma, which are favorable for the Sn decomposition.

First, a VHF plasma reactor was created and the process of tin decomposition and removal was investigated for basic parameters. As basic parameters, hydrogen gas pressure, hydrogen flow rate, Sn thin film and its ambient temperature were considered. We also investigated the possibility of efficient tin decomposition by combining VHF discharge with the hollow cathode effect to further increase the electron density.

It was unclear how hydrogen ion energy is involved when decomposing Sn thin films by ion reactive etching. Therefore, the device was modified so that a DC bias voltage could be applied to the Sn thin film. By this modification, the energy of the incident ions on the Sn thin film became variable in the range of 7-60 eV, and the dependence of hydrogen ion energy on Sn decomposition was investigated.

1.3 Outline of this thesis

The study is divided into five chapters, briefly summarized as follows:

Chapter 1 is the general introduction about the background to conduct this study and expound the formation of this thesis.

Chapter 2 includes three parts. The first part is introduction of the VHF plasma applied in this study to generate hydrogen radicals, and the Langmuir probe method to measure electron density and electron temperature. The second part is introduction of Sn transportation. The last part is diagnostic methods to

observe the surface change of samples by using SEM and to measure thickness of decomposed Sn film by XRF.

Chapter 3 describes detailed formation and characteristics of the compact VHF reactor applied in this study. Furthermore, a simple VHF hydrogen plasma was generated, and the efficiency and characteristics of Sn removal with respect to hydrogen gas pressure, gas flow rate, and sample temperature were investigated. Moreover, in order to examine the effect of hollow cathode, the reactor was rebuilt to generate hollow cathode discharge. Sn samples were Si substrates with an area of 15 × 15 mm^2 and thickness of 0.625 mm. The samples were covered by deposited Sn thin films, each with a thickness of approximately 100 nm. The decomposed Sn film thicknesses were quantitatively examined by XRF analysis. Efficiency of reactive ion etching for Sn removal is also discussed in this chapter.

Chapter 4 describes, experiments in which the dependence of the hydrogen ion energy on the Sn etching was investigated. Sn samples applied with various bias voltages were exposed to hydrogen plasmas. The etched thicknesses of the Sn films were quantitatively analyzed using XRF.

At last, chapter 5 is the summary of this study and the suggestion for future work.

References

[1] G.E.Moore, Int. Electron Devices Meet. 21, 11 (1975).

[2] F. Trintchouk, T. Ishihara, W. Gillespie, R. Ness, R. Bergstedt, C. Wittak and R. Perkins, Proc. SPIE 6154: 615423 (2006).

[3] K. Jain, C.G. Willson and B.J. Lin, IEEE Electron Device Letters. Vol.3 53–55 (1982).

[4] J. Miyazaki, A. Yen and J. Photopolym. Sci. Technol., Vol. 32, 2(2019).

[5] U.Stamm, I. Ahmad, I. Balogh, H. Birner, D. Bolshukhin, J. Brudermann, S. Enke, Frank Flohrer, Kai Gäbel, S. Götze, G. Hergenhan, Jürgen Kleinschmidt, Diethard Klöpfel, Vladimir Korobotchko, Jens Ringling, Guido Schriever, C. D. Tran and C. Ziener, Proc. SPIE 5037, 119 (2003).

[6] T. Higashiguchi, K. Kawasaki, W. Sasaki, and S. Kubodera, Appl. Phys.Lett. 88, 161502 (2006).

[7] K. Koshelev, V. Krivtsun, V. Ivanov, O. Yakushev, A. Chekmarev, V. Koloshnikov, E.Snegirev, and V. Medvedev, J. icro/Nanolithogr. MEMSMOEMS 11, 021103 (2012).

[8] Cutress, Dr Ian, "'Better Yield on 5nm than 7nm': TSMC Update on Defect Rates for N5". www.anandtech.com. Retrieved 2020.

[9] "Marvell and TSMC Collaborate to Deliver Data Infrastructure Portfolio on 5nm Technology". HPCwire. Retrieved 2020.

[10] J. S. Kim and J. Ahn, Electron. Mater. Lett., 14, 533 (2018).

[11] H.Mizoguchi, H. Nakarai, T. Abe, K. M. Nowak, Y. Kawasuji, H. Tanaka, Y. Watanabe, T. Hori, T. Kodama, Y. Shiraishi, T. Yanagida, T. Yamada, T. Yamazaki, S. Okazaki, T. Saitou, Proc. SPIE 9422, 94220C (2015).

[12] H. Mizoguchi, H. Nakarai, T. Abe, K. M. Nowak, Y. Kawasuji, H. Tanaka, Y. Watanabe, T. Hori, T. Kodama, Y. Shiraishi, T. Yanagida, T. Yamada, T. Yamazaki, S. Okazaki, T. Saitou, Proc. SPIE, 1009702 (2017).

[13] H. Mizoguchi, H. Nakarai, T. Abe, T. Ohta, K. M. Nowak, Y. Kawasuji, H. Tanaka, Y. Watanabe, T. Hori, T. Kodama, Y. Shiraishi, T. Yanagida, T. Yamada, T. Yamazaki, S. Okazaki, T. Saitou, Proc. SPIE, 867986790A (2013).

[14] R. Brainard, R. Brainard, E. Hassanein, J. Li, P. Pathak, B. Thiel, F. Cerrina, R. Moore, M. Rodriguez, B. Yakshinskiy, E. Loginova, T. Madey, R. Matyi, M. Malloy, A. Rudack, P. Naulleau, A. Wüest and K. Dean, Proc. SPIE 6923 (2008).

[15] E. Hassanein, C. Higgins, P. Naulleau, R. Matyi, G. Gallatin, G. Denbeaux, A. Antohe, J. Thackeray, K. Spear, C. Szmanda, C. N. Anderson, D. Niakoula, M. Malloy, A. Khurshid, C. Montgomery, E. C. Piscani, A. Rudack, J., A. Ma, K. Dean and R. Brainard, Proc. SPIE 6921 (2008).

[16] J. Biafore, M. D. Smith, E. van Setten, T. Wallow, P. Naulleau, D. Blankenship, S. A. Robertson and Y. Deng, Proc. SPIE 7636 (2010).

[17] H. Mizoguchi, T. Saito, N. Itou, T. Yamazaki, KOMATSU TECHNICAL REPORT, vol.62, 169(2016).

[18] A. A.Schafgans, D. J. Brown, I. V. Fomenkov, R. Sandstrom, A. Ershov, G. Vaschenko, R. Rafac, M. Purvis, S. Rokitski, Y. Tao, D. J. Riggs, W. J. Dunstan, M. Graham, N. R. Farrar, D. C. Brandt, N. Böwering, A. Pirati, N. Harned, C. Wagner, H. Meiling and R. Kool, Proc. SPIE 9422, 94220B (2015).

[19] E.R.Hosler, O. R. Wood II, W. A. Barletta, P. J. S. Mangat and M. E. Preil, Proc. SPIE 9422, 94220D (2015).

[20] M.M.J.W. van Herpen, D.J.W. Klunder, W.A. Soer, R. Moors, V. Banine, Chem. Phys. Lett. 484, 197 (2010).

[21] H. Meiling, V. Banine, N. Harned, B. Blum and P. Kurz, H. Meijer, Proc. SPIE 5751(2005) 90.

[22] V. Banine, R. Moors, Proc. SPIE 4343 (2001) 203.

[23] D. Ugur, A. J. Storm, R. Verberk, J. C. Brouwer, W. G. Sloof, Chem. Phys. Lett. 552, 122 (2012).

[24] D. Ugur, A.J. Storma, R. Verberk, J.C. Brouwer, W.G. Sloof, Appl. Surf. Sci. 288, 673 (2014).

[25] K. Tamaru, J. Phys. Chem. 60, 610 (1956).

[26] S. Hashiguchi and M. Hasikuni, Jpn. J. Appl. Phys., Part 1 26, 271 (1987).

[27] T. Lafleur and R. W. Boswell, Phys. Plasma 19, 023508 (2012).

[28] Paschen. F, App.Phys. 50, 901 (1916).

[29] J.P.Allain et al, Proc.SPIE 5751, Emerging Lithographic Technologies IX; (2005)

[30] D. T. Elg, J. R. Sporre, G. A. Panici, S. N. Srivastava, D. N. Ruzic, J. Vac. Sci. Technol. A, Vac. Surf. Film. 34, 021305 (2016).

[31] D. T. Elg, G. A. Panici, S. Liu, G. Girolami, S.N. Srivastava, D. N. Ruzic1, Plasma Chem. Plasma Process. 38, 223 (2018).

[32] C. Harvey, EPS Conference on Plasma Physics, P4.309 (2017).

Chapter 2 VHF Plasma Decomposition and Analysis Methods

2.1 Overview

In this study, we applied a 60 MHz VHF (very-high frequency) power supply to a CCP (capacitive coupled plasma) system [1]. Power is connected to one of two electrodes while another electrode is grounded. The electrons in the gas are accelerated by the VHF field and can ionized gas directly or indirectly by collisions, producing secondary electrons. When the electric field is strong enough, it can be lead to electron avalanche. After avalanche breakdown, the gas becomes electrically conductive due to free electrons. Generally, it accompanies light emission from excited atoms or molecules in the gas. Then visible light is produced, and plasma generation can be observed. In the CCP plasma system, one of the electrodes is connected to a matching box, which is actually a capacitor, and is electrically isolated. When high-frequency source is employed to the electrode, capacitor performs as a short circuit. Electrons impinge to the electrode through a sheath, and the electrode quickly obtains a negative charge or self-bias because the capacitor does not allow it to connect to ground. This sets up a secondary, DC field across the plasma in addition to the alternating current (AC) field. Massive ions are unable to follow the change of the AC field. Moreover, the constant and strong DC field accelerates ions toward the self-bias electrode. These energetic ions are utilized in various microfabrication process. One of the most representative application is reactive ion etching by setting target on the self-bias electrode. CCP plasmas have widely applied in the semiconductor processing industry for thin film deposition (such as sputtering and plasma-enhanced chemical vapor deposition) and etching.

Decomposition of Sn is based on the reaction of Sn atoms and hydrogen atoms to form SnH_4 and its exhausting with gas flow. The generated SnH_4 is unstable and easily decomposed into Sn which will readhere to the surface of substrate. Because the readhesion rate is related to temperature and pressure, we need to investigate transport and readhesion process of Sn. On the other hand, we also need to investigate the readhesion coefficient to know the real decomposition rate relying on all possible parameters.

Finally, the main measure methods in this study are SEM (scanning electron microscope) observation and XRF (X-ray fluoresce) analysis. The basement and application of these method are introduced at the last of this chapter.

2.2 Principle of VHF plasma and diagnostic technique

In this research we use VHF plasma to generate hydrogen atoms and we will introduce VHF plasma generation and electrons movements in the VHF electric field in the following contents. Moreover, the basement and application of Langmuir probe method in this study is also introduced.

2.2.1 VHF plasma

A VHF plasma is a kind of non-thermal plasmas which are produced at pressures ≦ 10 Torr. In the VHF plasma, electrons are heated up to a temperature of several eV, while ions and neutral particles remain at low temperatures which are close to the temperature of the chamber wall. This non-equilibrium feature is suitable for the plasma processing. The VHF plasma is characterized by electron trapping, that is, discharge frequency should satisfy the following condition:

$$f_{pi} << f < f_{pe} \qquad (2.1)$$

Here f is the discharge frequency, and f_{pi} and f_{pe} is the plasma frequency of ions and electrons, respectively. In addition, the electron displacement δ_x should be shorter than a spacing gap between discharge electrodes for $\omega << \upsilon_m$ [2]:

$$\delta_x = \frac{qE_0}{m_e \omega \upsilon_m} \ll \frac{d}{2} \qquad (2.2)$$

Here d is a spacing gap between discharge electrodes, ω and υ_m is the angular frequency of VHF power source and electron collision frequency, respectively, and q, me and E_0 is electron charge, electron mass and the amplitude of the VHF electric field. As shown in Fig.2.1, electron trapping effect provides better confinement of electrons and as a result the electron density becomes high. Thus, the electron density is considered to peak at a certain condition where electron trapping is most effective. The Eq. 2.2 indicates that E_0 and υ_m are important parameters in a VHF plasma, that is, the VHF power and pressure are key

parameters in the VHF plasma characteristics. When the VHF power is increased, the amplitude of the electron oscillation in the VHF electric field E_0 increases and as a result the condition for electron trapping, $\delta_x << d/2$, is not valid. Therefore, to increase υ_m by increasing the pressure is required for VHF plasma discharges at high powers.

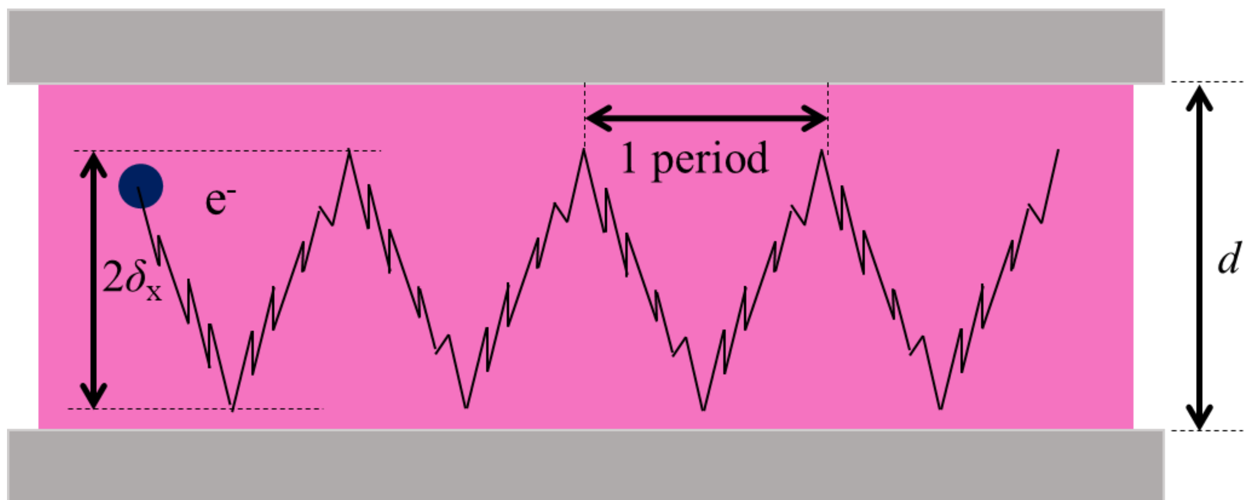

Fig. 2.1 Schematic diagram of electron motion in VHF electric field.

2.2.2 Langmuir probe method

The Langmuir probe is the simplest method to measure the plasma parameters. The most extensive use of the Langmuir probe is in the industry such as silicon thin film solar cells and semiconductors, where non-thermal plasmas are used for deposition and etching. Recently there is a tendency to produce plasma at high pressures to obtain high rates of deposition and etching. These partially ionized plasmas require special techniques in probe construction and theory.

When the potential applied to the probe V_p is much larger than the space potential V_s ($V_p >> V_s$), an electron current I_e is collected. Here, the probe current is negative. When $V_p << V_s$, an ion current Ii is collected. I-V curves are plotted as shown in Fig. 2.2.

As shown in Fig. 2.2, it can be divided into three main parts; ion saturation region (part A), transition region (part B), and electron saturation region (part C). The space potential (V_s) is near the bended point of the curve. At the part A (ion saturation region), where all the electrons are repelled, the ion saturation current (I_{sat}) is obtained. The Floating Potential (V_f), is where the ion and electron currents are equal, and the net current is zero. In the part A, the ion current is negligible, and the electrons are partially repelled by the negative potential $V_p - V_s$. In a Maxwellian plasma, the current increases exponentially in this part. When V_p reaches Vs, all of the electrons is collected. In the part I, I_e grows only slowly because of the expansion of the sheath. From I - V curve, the electron density ne, electron temperature T_e, and plasma potential V_s can be determined.

Hydrogen gas was used here and the gas pressure and the VHF power were 35Pa and 20 W, respectively. The dc bias voltage is varied from -50 V to +110 V while the DC current flowing to the probe measured. From Fig. 2.3, it can obtain much information what we introduced in above. From those, the plasma parameters, such as T_e and n_e can be estimated. The detailed procedure for calculating T_e and n_e are explained in the next paragraph.

Part B. is the transition region. When the I-V curve is plotted semi-logarithmically, the exponential part should be a straight line if the electrons have a Maxwellian velocity distribution function:

$$I_{\rm e} = I_{\rm es} \exp\left(-\frac{eV_{p-}V_s}{k_B T_{\rm e}}\right) \tag{2.3}$$

$$I_{\rm es} = \frac{1}{4} en_{\rm e}SV = en_{\rm e}S\sqrt{\frac{k_B T_{\rm e}}{2\pi m}} \tag{2.4}$$

where S being the surface area of the probe tip, k_B is the Boltzmann constant, and m is the ion mass. Here, I_{es} is the electron saturation current, or thermal current to a surface at Vs. Eq. 2.3 shows that the slope of the (ln I) − V_p curve is exactly $1/T_e$ and is a good measure of the electron temperature. We can obtain the electron temperature by the electron temperature. We can obtain the electron temperature by the equation as follows.

$$\frac{d\ln|I_{\rm e}|}{dV} = -\frac{e}{k_B T_{\rm e}} \tag{2.5}$$

Part A. Ion saturation region

In the part III on the probe curve of Fig. 2.2, the potential is sufficiently negative with respect to the plasma potential that only ions are collected by the probe. This is ion saturation current, and the total current is

$$I_{\rm is} = \frac{1}{4} en_{\rm i}Sv_i \tag{2.6}$$

where S is the area of the probe, n_i is the ion density, and v_i is the mean thermal velocity of ions that leave the plasma. Substituting the ion thermal velocity into Eq. 2.6 yields

$$I_{\rm is} = \frac{1}{4} en_{\rm i}S\sqrt{\frac{8k_B T_{\rm i}}{\pi M}} \tag{2.7}$$

where T_i is the ion temperature in K, and M the ion mass.

As well known, ions do not have a Maxwell distribution. Thus, in order to obtain the ion saturation current, we have to solve the sheath equation derived from the Poisson equation. According to the sheath

theory [5], the ion saturation current is expressed by

$$I_{\mathrm{is}} = \alpha_p e n_0 S \sqrt{\frac{k_B T_{\mathrm{i}}}{m_{\mathrm{i}}}} \qquad (2.8)$$

Setting Eq. 2.3 and Eq. 2.8 equal yields

$$V_{\mathrm{f}} = \mathrm{V}_s - \frac{k_B T_e}{2e} ln \frac{2M}{\pi m} \qquad (2.9)$$

The potential difference (V_{s}-V_{f}) is called the wall potential that corresponds to the ion bombardment energy. The theoretical value is α_{p} = exp (−1/2) = 0.61. We can estimate the electron density obtained from the ion saturation current by Eq. 2.10.

$$n_i[\mathrm{cm}^{-3}] = n_e[\mathrm{cm}^{-3}] = 2.56 \times 10^{23} \times \frac{I_{is}[\mathrm{mA}]\sqrt{m_i}[\mathrm{kg}]}{S[\mathrm{cm}^2]\sqrt{T_e}[\mathrm{eV}]} \qquad (2.10)$$

Part A. is the electron saturation region. Since the probe in electron saturation collects all electrons incident on the plasma sheath boundary, the total electron current collected by the probe is given as

$$I = I_e = \frac{1}{4}(e n_e S \mathrm{v}_e) = \frac{1}{4}(e n_e S)\sqrt{\frac{8 k_B T_e}{\pi m_e}} = I_{es} \qquad (2.11)$$

Where S is the surface area of the probe, ne is the electron density, v_{e} is the mean thermal velocity of the electrons, and me is the electron mass.

From Eq. 2.11, the electron density can be estimated from the electron saturation current.

$$\boldsymbol{n_{\mathrm{e}}} = \frac{\boldsymbol{I_{\mathrm{es}}}}{\boldsymbol{eS}}\sqrt{\frac{\boldsymbol{2\pi m_{\mathrm{e}}}}{\boldsymbol{k_B T_{\mathrm{e}}}}} \qquad (2.12)$$

Thus, we can estimate the electron density from the ion saturation current, Eq. 2.10, and the electron saturation current, Eq. 2.12. Theoretically, both should be the same. However, in the presence of magnetic fields and negative ions, the electron saturation current becomes lower than theoretical value, so that Eq. 2.10 is widely used to estimate the electron density. In this experiment, we estimated the electron density using Eq. 2.10.

The structure of the experimental setup and the probe tip is set at the center of the reactor. The probe

tip is made of a tungsten rod or wire having a diameter in the range from 0.1 to1 mm. The rod is insulated by a ceramic tube from the plasma except for a short length of exposed tip, about 10 mm long. These probe tips can be exposed to low-temperature plasmas without melting. To avoid disturbing the plasma, the ceramic tube should be as thin as possible, preferably < 1 mm in diameter. The assembly is encased in a vacuum jacket, which could be a metal steel or glass tube 1/4 in outside diameter. It is preferable to make the vacuum seal at the outside end of the probe assembly rather than at the end immersed in the plasma, which can cause a leak. Ideally, only the ceramic part of the housing should be allowed to enter the plasma. For this study, the area of the probe wire was 1.8×10^{-5} m^2 (the diameter of the tungsten is 0.5 mm, the length is 11 mm).

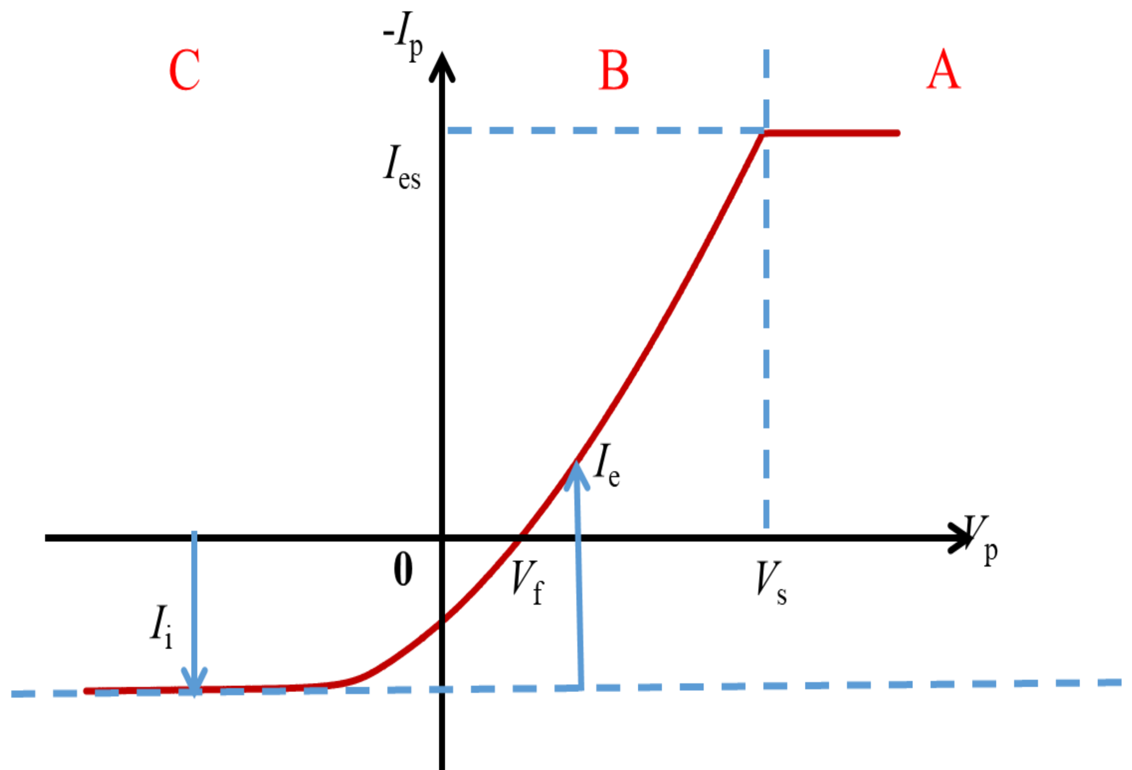

Fig. 2.2 Schematic of the *I*-*V* curve obtained by the probe method.

2.3 Principle of Sn decomposition

As it is referred in chapter 1, there are two basic methods to remove Sn deposition with hydrogen plasmas. First method is shown as the function of Fig. 2.15. One SnH_4 molecule is generated per 90000 incident H radicals when atomic hydrogen exposure of a Sn coated surface [6], comparing with the prepared investigation did before we suppose it takes a time less than one hour to decompose tin debris totally. One the other hand, the decomposition [7] of Sn debris is a fast-order reaction in respect to tin hydride, being independent of hydrogen pressure, and the activation energy of the reaction is 9.1kcal/mol between 100 ℃ and 35 ℃. The decomposition process does not proceed at a measurement rate on surface at 60 ℃.

$$Sn + 4H \rightarrow SnH_4 \uparrow \qquad (2.13)$$

Transportation of SnH_4 in a real EUV lithography reactor is indicated in Fig. 2.3. The ionized Sn adheres on the condenser mirrors merged by the reaction of laser produced plasma and hot Sn droplets. In order to remove Sn adhesion, hydrogen gas of approximately 10 Pa is fulfilled in EUVL reactor. Hydrogen molecules are dissociated by EUV light (photon energy 92 eV) hydrogen atoms react with Sn atoms forming volatile gas SnH_4, which is exhausted by hydrogen gas flow. For another method, hydrogen plasma is generated by VHF source, and hydrogen ions are employed to decompose Sn debris. This process supposed to be a reactive ion etching.

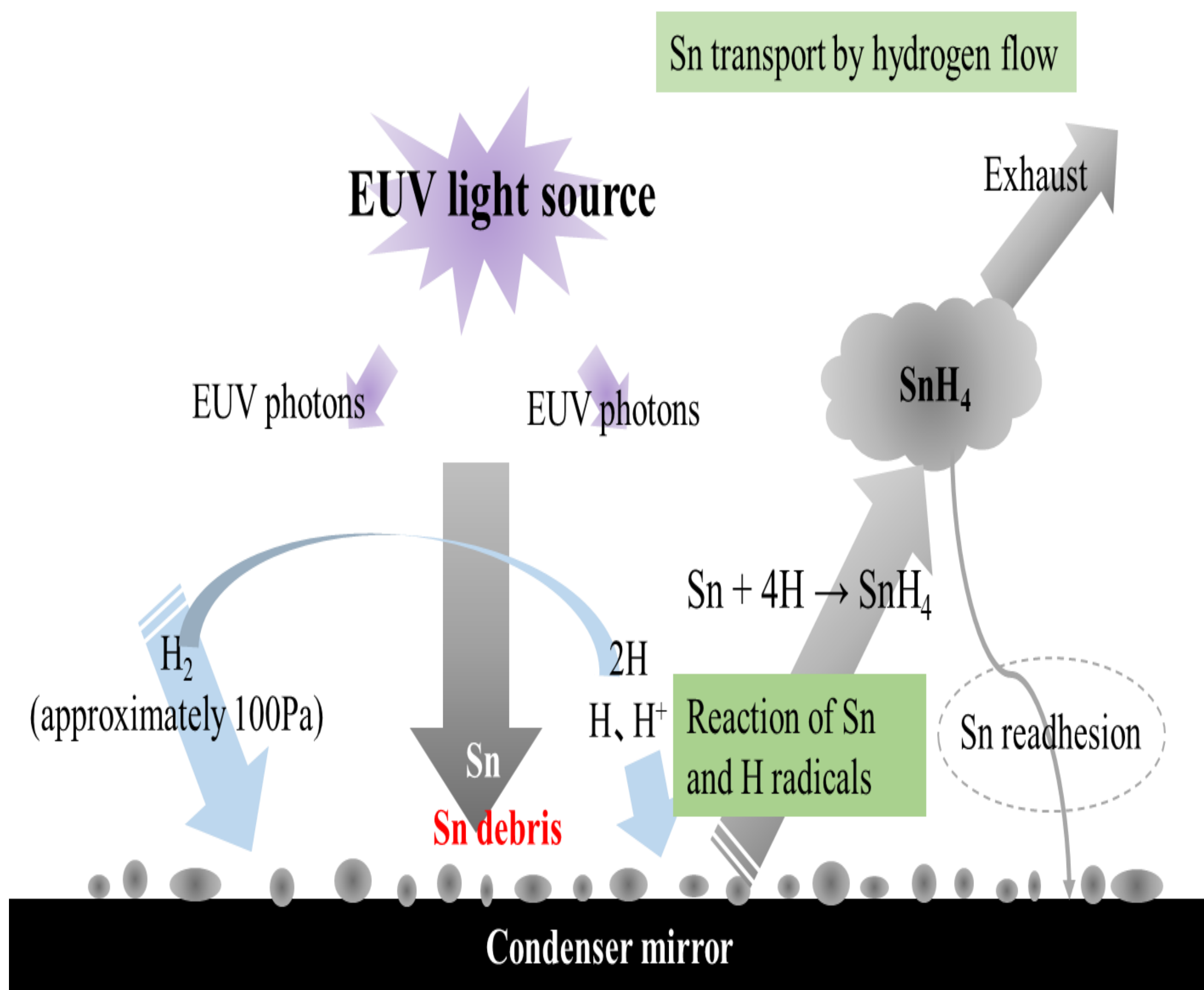

Fig. 2.3 Images of Sn decomposition based on hydrogen radicals and hydrogen ions

To investigate the velocity of hydrogen molecules flow in the reactor. The calculation as following is performed. Firstly, we need to know the density of hydrogen molecules in the reactor, here ideal gas law $PV = nkT$ is applied to Eq.2.13, where k is Boltzmann constant.

$$n = 7.24 \times 10^{22} \times \frac{p}{T} \tag{2.14}$$

The number of hydrogen particles N passing through the cross section in a second is calculated as Eq.2.14, here q is hydrogen gas flus.

$$N = n \times \frac{q}{60} \times 10^{-6} \tag{2.15}$$

When temperature is 0°C and the hydrogen gas pressure is 1 atm, the number of hydrogen particles N can be obtained as Eq.2.15.

$$N = 7.24 \times 10^{22} \times \frac{10^5}{273} \times \frac{q}{60} \times 10^{-6} = 4.42 \times 10^{17} \times q \tag{2.16}$$

The time a hydrogen molecule need to pass through the reactor is shown as Eq.2.16.

$$t = \frac{50 \times 10^{-3}}{v} \tag{2.17}$$

And the number of hydrogen molecules remain inside of reactor can be calculated by Eq.2.17 with the results obtain from Eq.2.18 and Eq2.19.

$$N_S = N \times t = 4.42 \times 10^{17} \times q \times \frac{50 \times 10^{-3}}{v} = 2.21 \times 10^{16} \times \frac{q}{v} \tag{2.18}$$

The volume of hydrogen molecules pass through reactor indicate as Eq.2.18.

$$V = (15 \times 10^{-3})^2 \times 50 \times 10^{-3} = 1.13 \times 10^{-5} \tag{2.19}$$

Therefore, the number N_s of hydrogen molecules in the chamber can be expressed as follows from Eq.2.13 and Eq.2.18.

$$N_S = n \times V = 7.24 \times 10^{22} \times \frac{p}{T} \times 1.13 \times 10^{-5} = 8.18 \times 10^{17} \times \frac{p}{T} \tag{2.20}$$

Moreover, the flow velocity of hydrogen gas in the chamber is determined by comparing Eq.2.15 and Eq.2.20.

$$N_S = 2.21 \times 10^{16} \times \frac{q}{v} = 8.18 \times 10^{17} \times \frac{p}{T} \tag{2.21}$$

In addition, velocity of hydrogen molecules inside of the reactor shows as Eq.2.22.

$$v = 2.70 \times 10^{-2} \times \frac{qT}{p} \tag{2.22}$$

The reaction in which SnH_4 is produced by the reaction between a hydrogen atom and tin debris is expressed by Eq. 2.13. The temperature dependence of the reaction rate constant in this reaction can be shown in Figure 2.4, reported by Tamaru [10]. It can be seen that the reaction rate constant decreases as the temperature decreases, and that it changes exponentially with respect to the reciprocal of the temperature. Therefore, it is considered that the lower the temperature of the mirror, the more the generation of SnH_4 is promoted and the decomposition of SnH_4 is hindered, so that the amount of tin taken on the surface of substrate increases.

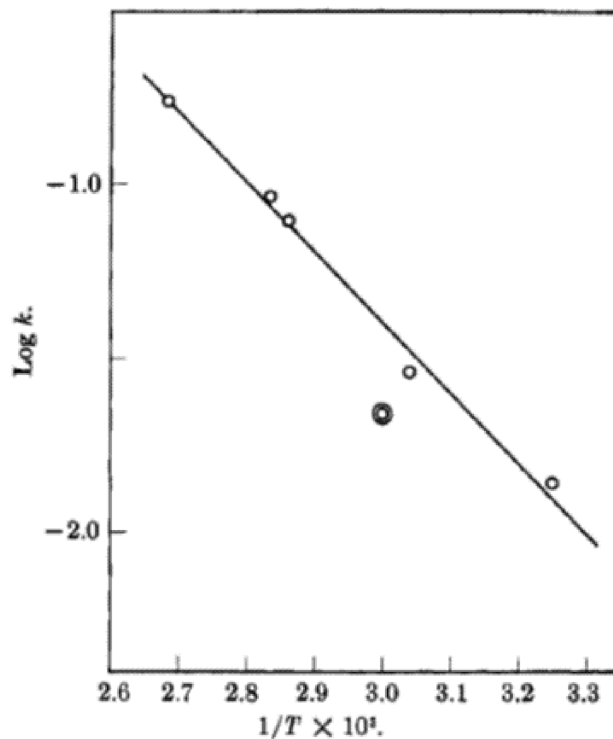

Fig. 2.4 Dependence of rate constant upon temperature [10].

2.4 Analysis methods

In this study we use XRF analysis and SEM observation to evaluate samples quantitatively and qualitatively, respectively. Both EDX analysis and XRF analysis rely on interaction of X-ray and a sample, as the basement X-ray is photons of electromagnetic radiation, like light, radio waves, and at the other end of the spectrum γ-rays [14]. They are distinguished by their wavelength range, generally about 0.1 to 100 angstroms, and their origin from events in the structure of atoms. X-rays penetrate much further through ordinary things than visible lights do, and this means that images formed with X-ray can be used to reveal internal structure.

XRF (X-ray fluorescence) relies on the use of X-ray or gamma ray photons to produce excited atoms, which in turn emit characteristic X-ray, is in many respects quite different from the use of electrons or other charged particles. The cross section for stopping (absorbing) the incoming photon is different, and this produces a different depth distribution of excitation, which in turn gives rise to different absorption and fluorescence effects for the generated X-ray. Also, the background in the measured spectrum is quite different because the photons cannot directly produce braking radiation. These effects, and some of the consequences for a mathematical model of the intensity-concentration relationship, will be dealt as following. It is useful to recall that in the great majority of instruments that perform X-ray fluorescence measurements, the excitation is produced by X-ray which are themselves generated by electrons. The conventional X-ray tube is simply a rather specialized electron beam, which an accelerating voltage of perhaps 10 to 60 keV (some systems go higher or lower, and dental or medical X-ray tubes and generators are often over 100 keV to produce higher energy X-ray which will penetrate further). The target in the tube emits X-ray or braking radiation covers all energy up to the maximum voltage on the tube, and on the top of that are the characteristic emission lines from the elements in the target. It is most common to select target element based first and foremost on their electrical and thermal properties, because the tube may operate at power levels of several kV, much higher than the power level in even an electron microprobe. The heat generated in these high power tubes is usually removed by a water circulation system, but even so, since the depth of penetration of the electrons is very small (compared

to the thickness of the target or anode), the heat conductivity is important, and so is the ability of the target to maintain its integrity at somewhat elevated temperatures. Refractory metals are, however, not good thermal conductors. The usual arrangement is to make the anode assembly out of copper, and apply a thin coating of the element to be used as a target. The detector formation of a XRF analysis is indicated as Fig. 2.5.

The result of XRF analysis indicates by analysis lines which are selected on the basis of intensity, accessibility by the instrument and lack of line overlaps. Table 2.1 shows the wavelengths and typical lines used of elements in this study.

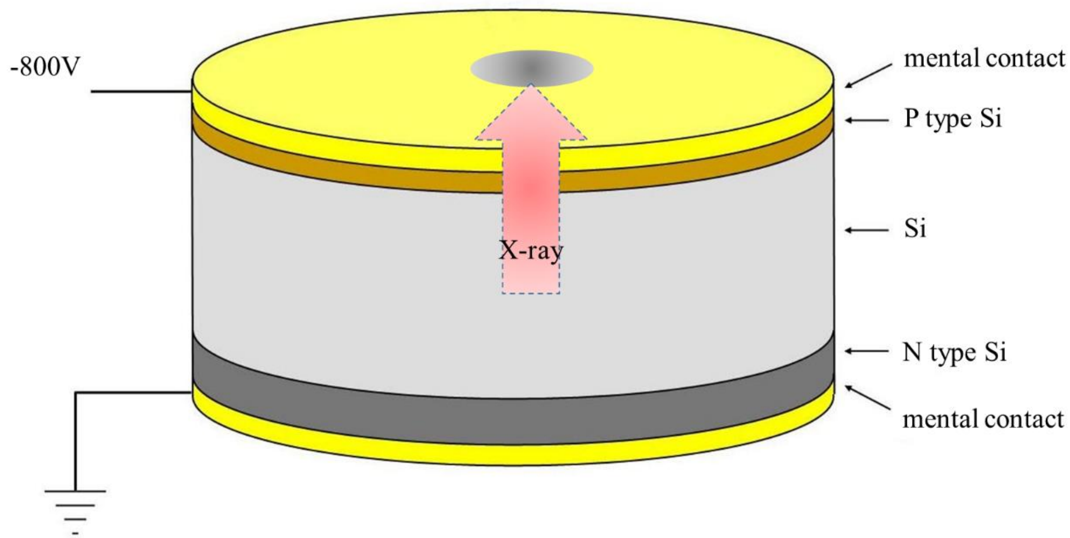

Fig. 2.5 Schematic form of a XRF detector

element	line	wavelength(nm)
Si	$K\alpha_{1,2}$	0.7126
Sn	$L\alpha_1$	0.3600

Table 2.1 Wavelengths and typical lines used of common elements

A scanning electron microscope (SEM) is a kind of electron microscope scans the surface of sample with a focused beam of electrons to produce images. Information about surface topography and composition of a sample delivers by various signals produced by the interaction of electrons and atoms in the sample. The electron beam is scanned in a raster scan pattern producing a new image via position of the beam combine with the detected signal. SEM can display image even smaller than 1nm.

The principle of SEM operation can be conclude as a finely pointed electron beam (of diameter<10nm) scans the sample point by point and line by line. At the same time, the electron beam of a cathode ray tube scans the display surface synchronously with the electron beam scanning the sample. The incidence of the electron beam at a point on the sample gives rise to emitted electrons, which are of two types: secondary electrons and back-scattered electrons. The brightness of the corresponding point on the display tube is controlled by the amount of emitted electrons. Points on the sample which gives rise to large quantities of emitted electrons therefore give bright points on the display tube and points on the sample where the quantity of emitted electrons is low show up as dark points. Intermediate values give finely divided shades of grey on the display tube. Figure 2.6 shows the image of SEM observation took at the center point for the surface of a sample.

In the SEM observation, the specimen area on which the electron beam is incident emit X-rays are used for the analysis of the elements contained in the sample. There is a detector system which can detect and indicate the relative intensities of the characteristic radiation emitted, it is EDX. SEM is used for the element analysis and chemical characterization of a sample, relying on some source of X-ray excitation interact with a sample. Because in a large part to the fundamental principle that each element has a unique set of peaks on its electromagnetic emission spectrum [15], ensuring the characterization capabilities.

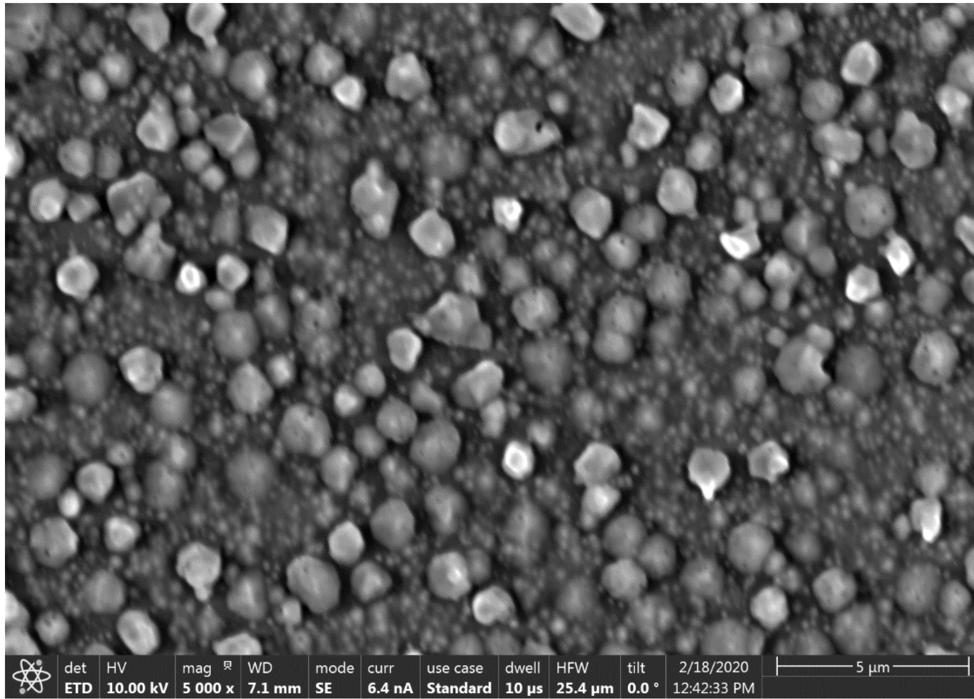

Fig. 2.6 Image of SEM observation on the surface of a sample.

References

[1] UK Wireless Telegraphy (Short Range Devices) (Exemption) Regulations 1993.

[2] S. C. Brown, Introduction to Electrical Discharges in Gases, Chap.10 (John Wiley & Sons, 1966).

[3] M. A. Lieberman and A. J. Lichtenberg, Principles of Plasma Discharges and Materials Processing, Chap.4 (John Wiley & Sons, 1994).

[4] Francis F. Chen, John D. Evans, and Donald Arnush, Phys. Plasmas, Vol. 9, 4 (2002).

[5] Park SK, Economou DJ, et al, J Appl Phys, 66(7):3256–3267 (1989).

[6] D. Ugur, A.J. Storm, R. Verberk, J.C. Brouwe, W.G. Sloof, Chemical Physics Letters 552 122–125 (2012).

[7] Elg DT, Panici GA, Peck JA, Srivastava SN, Ruzic DN J., Micro/Nanolithogr MEMS MOEMS 16(2):23501 (2017).

[8] Park SSKS, Economou DJ, et al, J Electrochem Soc, 137(8):2624–2634 (1990).

[9] Zhang P, Hu L, Meegoda JN, Gao S, Micro/nano-pore network analysis of gas flow in shale matrix. Sci Rep 5(1):13501 (2015).

[10] Tamaru K , J Phys Chem 60(5):610–612 (1956).

[11] Elg DT, Panici GA, Peck JA, Srivastava SN, Ruzic DN Modeling , J Micro/Nanolithogr MEMS MOEMS 16(2):23501 (2017).

[12] Park SK, Economou DJA, J Appl Phys 66(7):3256–3267 (1989).

[13] Greenwood, Norman N.; Earnshaw, Alan, Chemistry of the Elements (2nd ed.). Butterworth-Heinemann. ISBN 0-08-037941-9 (1997).

[14] T. Nishimiya, Y. Takeuchi, Y. Yamauchi, H. Takatsuka, T. Shioya, H. Muta, Y. Kawai, Thin Solid Films 516, 4430, (2008).

[15] Lothar Engel, Hermann Klingele. An Atlas of Metal Damage Surface examination by scanning electron microscope. Wolfe Science Books in association with Carl Hanser Verlag, Munich, Vienna.

Chapter 3 Investigation of Basic Characteristics of Sn Thin Film Decomposition

3.1 Introduction

Semiconductor devices are becoming more and more highly integrated. Therefore, a 7 nm node semiconductor process using EUV (Extreme Ultra-Violet) lithography has been started [1]. The EUV lithography light source uses the resonance line (wavelength 13.5 nm) of Sn polyvalent ions from high-temperature and high-density Sn plasmas obtained by irradiating Sn droplets with a CO_2 laser. At that time, Sn debris is generated from the Sn droplets and adheres to the EUV condenser mirror, which causes a problem of lowering the reflectance of the mirror. Although 250 W EUV light sources have already been commercialized [2,3], it is necessary to further increase the output in the future, and the problem of debris removal will become even more important.

As a countermeasure, it has been proposed to react Sn debris with hydrogen atoms to generate volatile gas SnH4 and remove it from the mirror surface [4]. In an actual EUV light source device, the chamber is filled with hydrogen gas of about 10 Pa, and hydrogen molecules are dissociated and ionized by EUV light (photon energy 92 eV). Finally, hydrogen atoms are reacted with Sn atoms to generate SnH_4, and SnH4 is exhausted together with hydrogen gas [5,6]. As a study of the Sn removal process, Ugur et al. investigated the decomposition of Sn through a chemical reaction using a hydrogen atom flux generated by dissociating hydrogen molecules with a hot filament [7,8]. As a result, it was reported that one Sn atom was removed for every 100,000 hydrogen atoms.

As another method, it was considered to generate a hydrogen plasma and efficiently remove Sn by RIE (Reactive Ion Etching) using the energy of hydrogen ions. In that method, Elg et al. reported that SnH_4 generation was promoted by breaking the bond between metal Sn atoms with the energy of hydrogen ions [9,10]. In that study, RF (radio frequency: 13.56 MHz) power was supplied to the powered electrode to irradiate the Sn thin film on the electrode surface with hydrogen ions. Hydrogen ions were accelerated through the cathode sheath by the negative bias voltage (-300 V) appearing on the electrode

surface. As a result, hydrogen ions obtained energy of approximately 300 eV. Elg et al. have achieved a Sn etching rate of 1.7 nm/min. However, Elg et al. concluded that Sn etching was independent of gas flow rate and surface temperature, and readhesion was negligible.

Because we have already investigated the dependence of Sn removal on hydrogen ion energy [11]. Bias voltages from -50 V to +7.5 V were applied to a Si substrate on which a thin film of Sn is deposited (hereinafter, Sn sample) exposed to hydrogen plasma to change the hydrogen ion energy. As a result, it has been clarified that the number of Sn atoms removed per hydrogen ion is maximized with hydrogen ion energy of approximately 10 eV.

As for the hydrogen plasma generation method, a higher density plasma can be obtained by using a VHF (very high frequency, 30-300 MHz) power supply. In this study, the possibility of using VHF plasma for Sn removal was investigated. By placing a Sn sample on the ground electrode, the voltage of the ion sheath becomes about 10 V, and it is expected that RIE will proceed with maximum efficiency as described above. In this study, we first clarified the basic Sn removal characteristics by VHF plasma using three variable parameters: hydrogen gas pressure, hydrogen gas flow rate, and Sn sample temperature. Furthermore, we investigated the possibility of realizing efficient Sn removal using RIE by combining VHF discharge with the hollow cathode effect to further increase the electron density [12,13].

3.2 Experimental Setup

A schematic diagram of the experimental equipment is shown in Fig. 3.1 (a) and (b). In Fig. 3.1 (a), VHF plasma was generated in the entire chamber, and the Sn removal characteristics of the basic VHF plasma were investigated in this arrangement. A 60 MHz VHF power supply was connected to the top electrode to power the device. The inner diameter of the quartz glass tube in the discharge space was 62 mm, and a Sn sample for Sn removal experiments was installed at the bottom of the chamber (earth electrode) and fixed with a stainless steel holding plate (thickness 0.1 mm) and screws. The Sn sample is a 100 nm thick Sn film deposited on the surface of a silicon substrate with an area of 15mm × 15 mm and a thickness of 0.625 mm. The Sn film has the same potential as the ground electrode through the

holding plate. The port for introducing hydrogen gas and the port for exhausting hydrogen gas were arranged in a straight line, most of the hydrogen gas flowed above the sample and the generated SnH_4 molecules were carried away by this flow. The vacuum vessel was evacuated to a pressure of 7×10^2 Pa using a turbo molecular pump. Constant temperature water was flowed inside the ground electrode to control the temperature. The Sn sample was brought into close contact with the ground electrode, and the temperature of the Sn sample was also controlled. The power supply was used in the output range of 20 W to 30 W.

As shown in Fig. 3.1 (b), the vacuum vessel was divided into an upper space and a lower space by a partition metal plate which was at a ground voltage, and a structure having a hollow cathode effect was created in the center of this partition metal plate. The side wall of the upper space was a quartz glass tube, and the height of the space was 30 mm. The VHF plasma was generated in this upper space. The lower space had an inner diameter of 56 mm and a depth of 16 mm and was surrounded by stainless steel surfaces and a partition metal plate. That is, the entire surrounding surface was at the ground voltage. A metal cylinder with an inner diameter of 16 mm and a height of 19 mm was attached to the center of the partition metal plate. The Sn sample was placed on the bottom surface just below the cylinder. In addition, 20 or more holes with a diameter of 3 mm were made in the partition metal plate around this cylinder so that hydrogen gas introduced from the side surface of the lower space could be supplied to the upper space as well. The hydrogen plasma generated in the upper space was ejected into the lower space through the cylinder in the center of the partition metal plate. The inside of this cylinder ca used the hollow cathode effect, and the Sn sample was irradiated with hydrogen plasma having a higher electron density than that of VHF plasma alone. Hollow cathode discharge did not occur in the holes with a diameter of 3 mm.

XRF (X-Ray Fluorescence) and SEM (Scanning Electron Microscope) were used for the evaluation of Sn removal. The device used for XRF analysis was Shimadzu EDX800. The actual film thicknesses of the Sn samples were measured by the crystal oscillator method. They were used for calibration during XRF analysis. Before and after the experiment, the amount of Sn in the Sn sample was detected as a

SnL_{α} signal and converted to film thickness. At the center of the sample, changes in the state of the Sn film surface were observed by SEM.

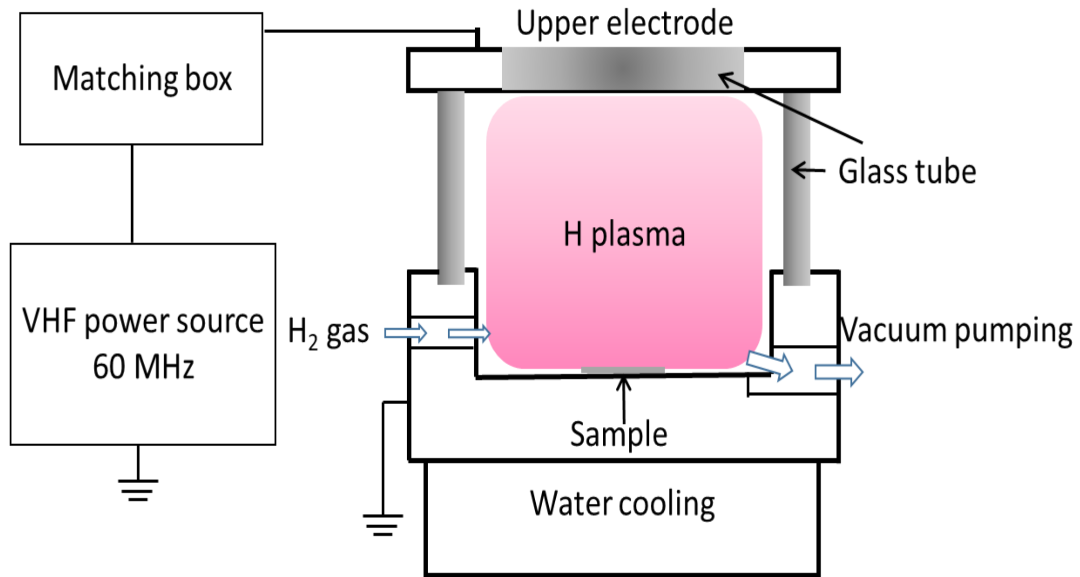

(a)

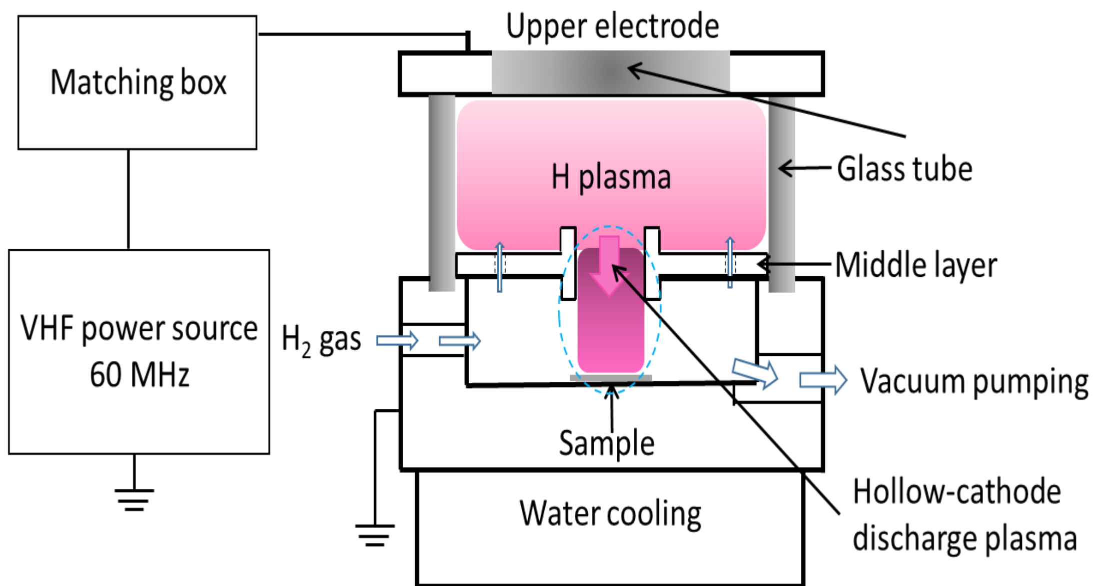

(b)

Fig. 3.1 Schematic of experiment system.

3.3 Results and discussion

Firstly we have performed Langmuir probe method to measure the plasma density and plasma temperature in these experiment for different gas pressure and gas flow rate. The results of probe was measured with gas flow rate while source power was fixed at 20 W and the gas pressure at 35 Pa. When gas pressure was 35 Pa, the average electron density was n_e =2.8×10^{15}m^{-3} and electron temperature was T_e=2.6 eV. Furthermore, the basic parameters matter in this study are gas pressure, gas flow rate and temperature, the dependency of these parameters are shown as the following sections.

To evaluate the decomposition process qualitatively we performed SEM observation on the center area of the surface for each sample. It is found when the decomposed thickness of Sn film is much than half of the total thickness (50mm), the evaluation of thickness variation becomes non-linear which is unable to analysis. In the following part only the cases that decomposed thickness less than 50mm are discussed. The results of SEM observation for the surface of substrates which were magnified by 5000 times are shown as the following figures. Fig. 3.2 indicates the surface of substrate did not expose to hydrogen plasma, the dark-brown Sn film distributes on the surface uniformly and black silicon base can barely see.

Figure 3.3 and 3.4 show the results of SEM observation for surface which were magnified by 5000 times of samples expose to plasma for 10min and 20min, respectively. (a) is the result for 15 Pa, the shape of Sn remaining became smaller and black areas increased, it shows VHF hydrogen can definitely decompose Sn. (b) is the result for 35Pa, the shape of Sn remaining furtherly decreased, and the silicon base are farther clearly than the case of 15Pa. (c) is the result for 75 Pa, the shape of remaining increased while the black silicon base decreased, the surface was became white than the cases of lower gas pressure. And much island-shape contaminant can be observed. It is supposed that readhesion had happened. (d) is the result for 150 Pa, the island-shape contaminant was further significantly, the readhesion of Sn was promoted at high gas pressure.

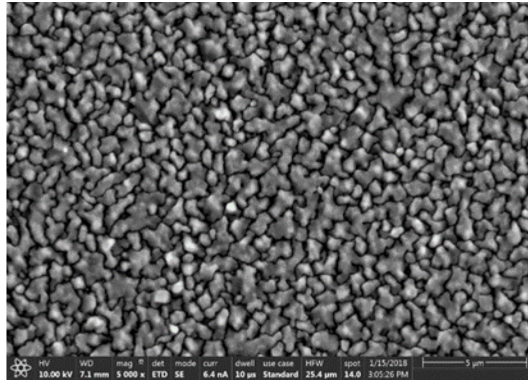

Fig. 3.2 Reference (substrate without plasma exposure).

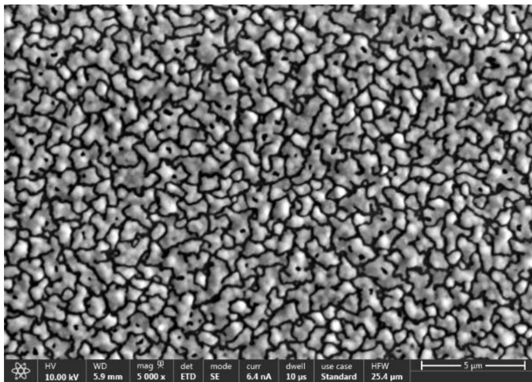

(a) P_{H2} = 15Pa

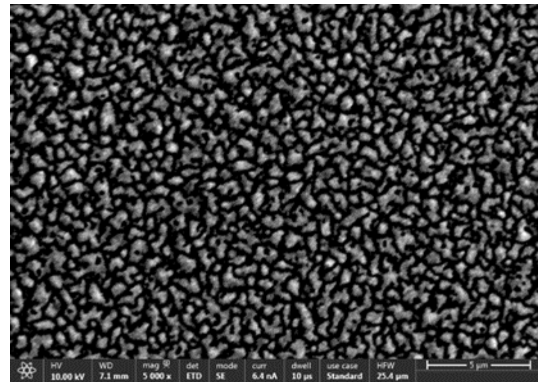

(b) P_{H2} = 35Pa

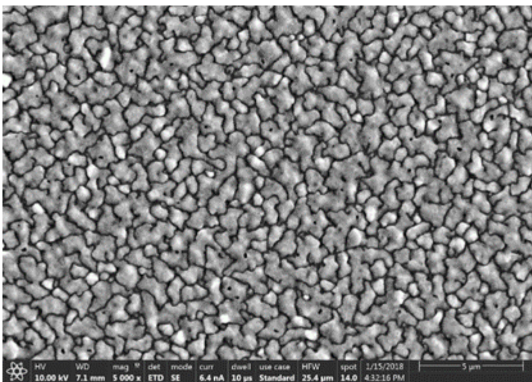

(c) P_{H2} = 75Pa

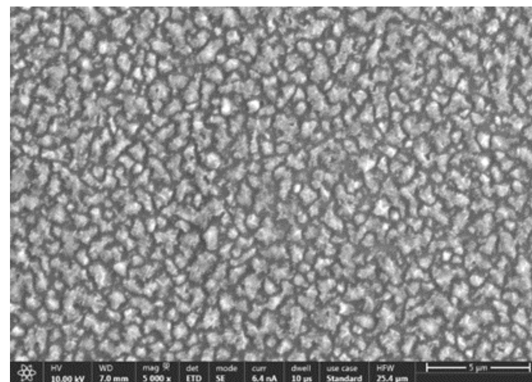

(d) P_{H2} = 150Pa

Fig. 3.3 SEM observation for surface of samples expose to plasma for 10min.

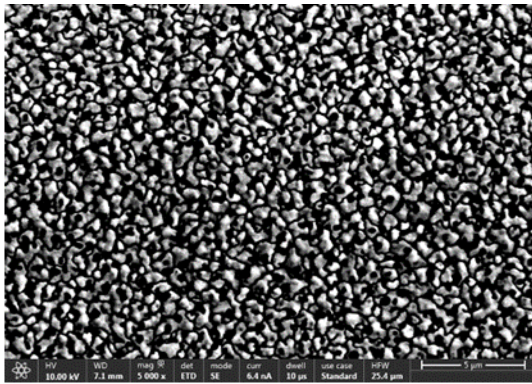

(a) P_{H2} = 15Pa

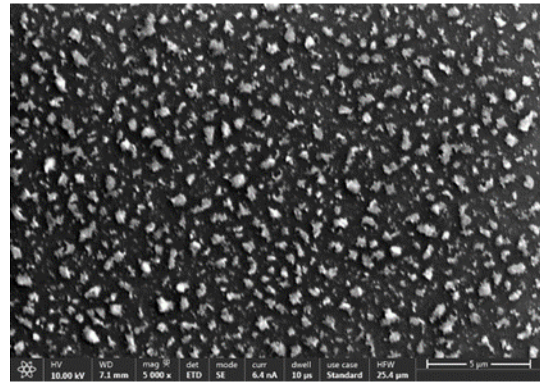

(b) P_{H2} = 35Pa

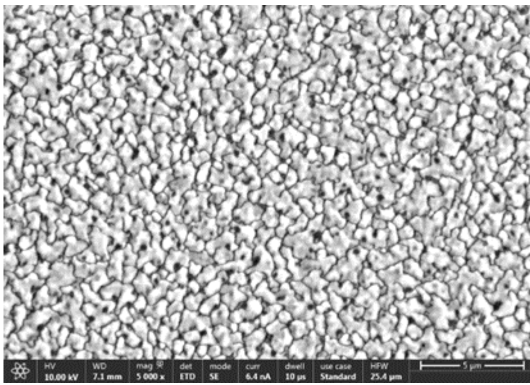

(c) P_{H2} = 75Pa

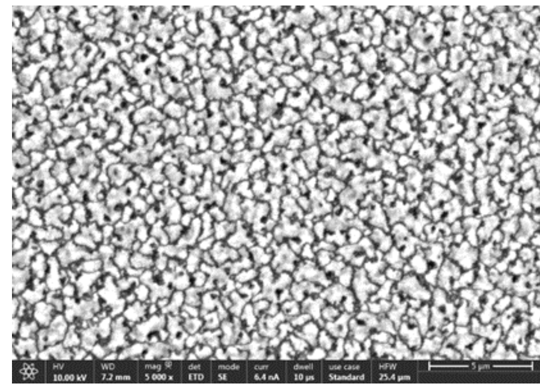

(d) P_{H2} = 150Pa

Fig. 3.4 SEM observation for surface of samples expose to plasma for 20min

To investigate dependence of gas pressure we have performed experiments at 15 Pa, 35 Pa, 75 Pa and 150 Pa. Gas flow rate was fixed at 20 sccm, temperature was 20 ℃ and power source was 20 W. The exposure time to plasma were 10, 20, 30 and 40 min, respectively.

Figure 3.5 and 3.6 show the results of Sn film thickness quantitatively measured by XRF analysis depended on gas pressure for 10 min and 20 min, respectively. It can be seen both in the case of 10 min and 20 min, when the gas pressure at 35 Pa decomposed thickness of Sn film is most high. It can be considered that the hydrogen flux is larger than the case of 15 Pa. Furthermore at the cases of 75 Pa and 150 Pa, readhesion was formed on the surface of substrate for the mean free path became shorter while the gas pressure increased. Collisions between Sn atoms and hydrogen atoms were frequently when mean free path is shorter. Consequently, 35 Pa was the most efficient gas pressure for Sn film decomposition. Thus, the peak etching rate in this study can be calculated as 4.8nm/min, which is higher than the result reported by the study made by Elg [9,10] as 1.7 nm/min. The efficiency of the VHF plasmas to clean the Sn decomposition have been proved with the VHF reactor applied in this experiment.

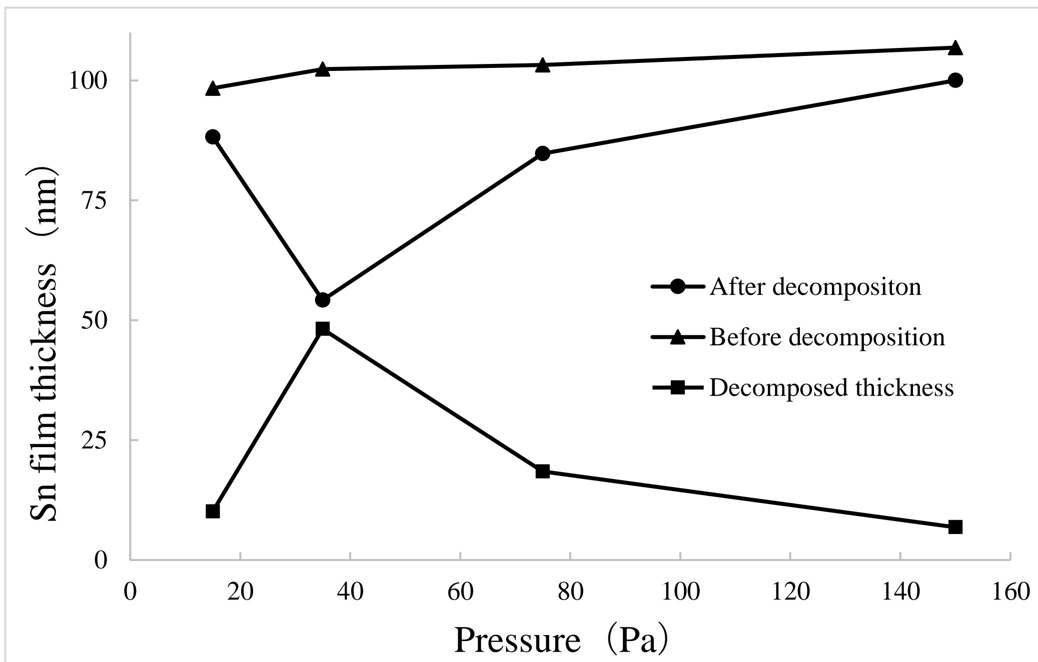

Fig. 3.5 Dependence of Sn removal on gas pressure measured for 10min.

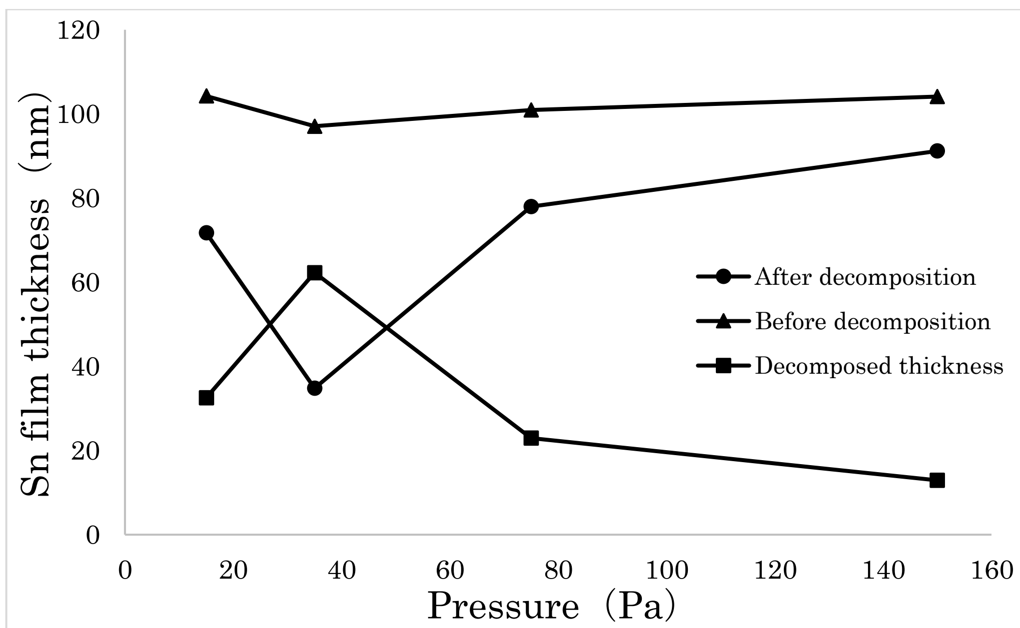

Fig. 3.6 Dependence of Sn removal on gas pressure measured for 20min.

Fig. 3.7 shows the dependence of Sn film thickness on gas flow rate measured for 30min. To investigate the dependence on gas flow rate, gas pressure was fixed at 50 Pa, temperature was 20 ℃ and power source was 20 W. Gas flow rate was varied as 20, 40, 60 and 80sccm. It can be seen from the figure to the decomposed thickness that although the variation was not linear, the value of decomposed thickness increased while the gas flow rose. However, at the case of 60 sccm and 80 sccm decomposed thickness was more than 50mm, the results lost reliability for the remaining is less than the range of analysis. Decomposition of Sn film was promoted gas flow rate increased, gas flow rate has positive effect in this process.

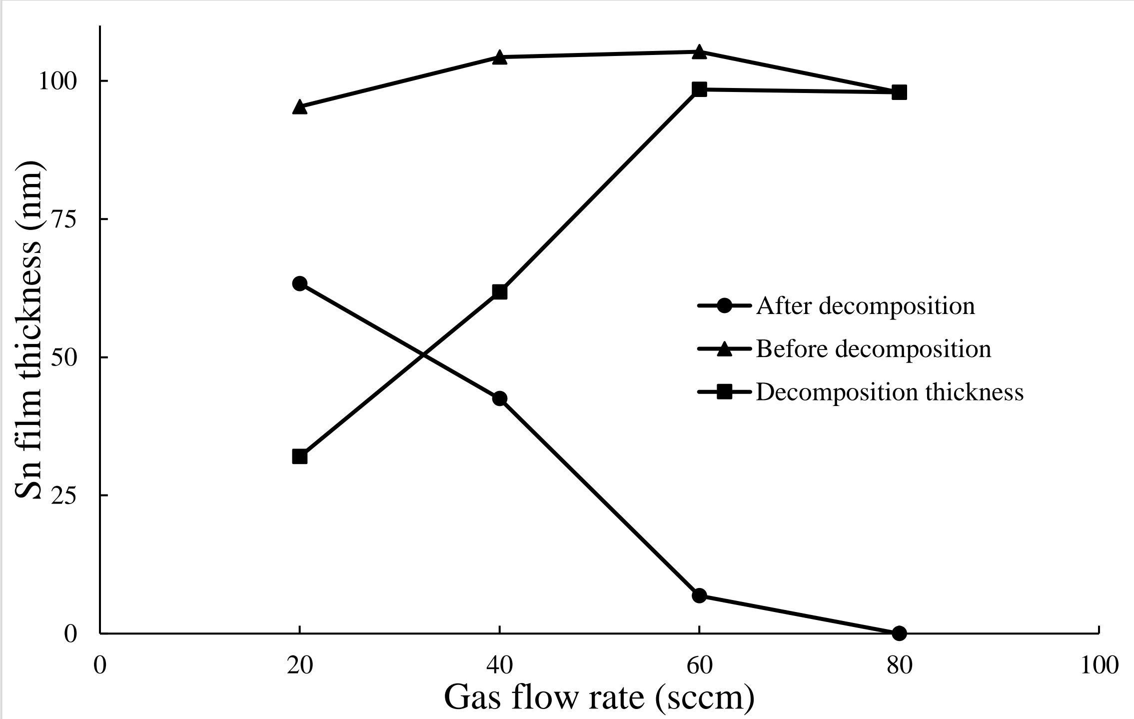

Fig. 3.7 Dependence of Sn removal on sample surface temperature measured for 30min at 60sccm.

In this experiment we have investigated the dependency of 20, 40 and 60 °C, respectively, at the gas flow rate at 80 sccm. According to Tamaru [14] the dissociation rate coefficient of SnH_4 increases by one order when gas temperature increases 60 °C, it is necessary to investigate the temperature dependence at least up to 60 ℃. Figure 3.8 shows the dependence of Sn removal on Sn sample temperature. For the dissociation rate coefficient of SnH_4 increased, readhesion was significantly than decomposition rate while the temperature increased. In this case 20 ℃ was the most efficient temperature for Sn decomposition, it is supposed that lower temperature can avoid readhesion which is proper in decomposition process.

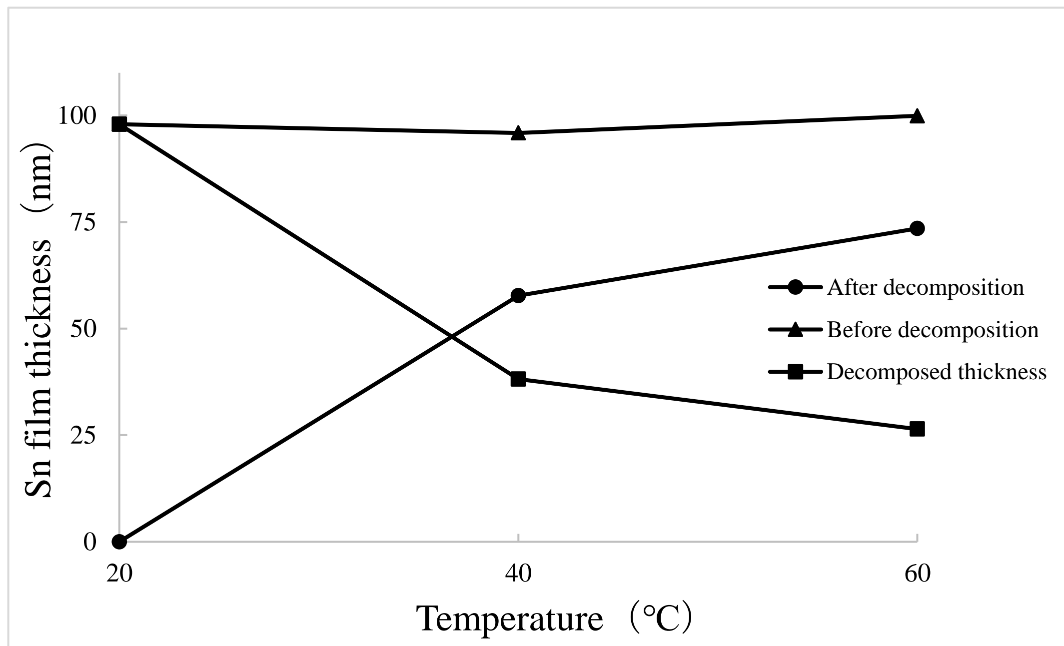

Fig. 3.8 Dependence of Sn film thickness on temperature measured for 30min at 80sccm.

During the decomposition process, ion sheath formed over the silicon substrate. Under the conditions of this experiment, the hydrogen ion was H_3^+ [15]. Based on the sheath theory [16] hydrogen ions were accelerated for the sheath potential and hydrogen ions acquired kinetic energy which was three time than the electron temperature. The electron density was $n_e = 2.8\times10^{15}$ m^{-3} and electron temperature was T_e=2.6 eV measured by Langmuir probe. The ion energy bombard the surface can be calculated as 7.8 eV. For the peak etching rate in this study was the case for gas pressure at 35 Pa, which was 4.8 nm/min. we can estimate the ion flux impinging on the surface using Eq. 3.1 which is known as the Bohm flux.

$$\Gamma_{\mathrm{i}} = 0.61 \times n_e \times \sqrt{\frac{\mathrm{k}_B T_e}{m_i}} \tag{3.1}$$

where k_B is Boltzmann constant and m_i is the mass of H ion. Using the values of T_e and n_e, we estimate the ion flux as $\Gamma_i = 2\times10^{19}$ m^{-2}/s. For the solid Sn, the density is n=7×10^3 kg/m^3. The thickness of the Sn thin film is d =4.8×10^{-8} m. Using the mass of Sn, we estimate the Sn atomic number in the unit area to be 1.7×10^{21} m^{-2}. The exposure time was 10min (35 Pa case), therefore the total ion fluence for 10 min is 8.5×10^{21} m^{-2}. That is, the Sn yield is 0.20. In other word, five hydrogen ions remove on Sn atom. At the chapter 1, we referred that, according to the report by D. Ugur [8], 90 thousand of H atoms are necessary to remove 1 Sn atom. Therefore, our reactor is more than 12000 times more efficient to remove Sn atoms.

In the pre-investigation experiment it was found that thickness of Sn film was varied spatially for the effect of hollow-cathode discharge. To a 15 mm × 15 mm square substrate, it was divided to three parts for each 5mm length from the gas inlet side as upstream area, middle stream area and downstream area. The hole on the bottom of chamber (which is same to the ground electrode) is near the downstream of the substrate, while the decomposed thickness of Sn film for downstream was approximately twice than those at other position of the substrate. A deep hole in the cathode, as shown in Fig. 3.9, induces a hollow cathode discharge. Electrons in the cathode hole are repelled by a potential well formed by ion sheaths in front of the hole walls [13]. This way, electrons are trapped in the hole and create a high density plasma through electron impact ionizations of neutral particles in the hole.

In order to investigate the promotion of Sn removal by adding the hollow cathode effect to VHF hydrogen plasma, a Sn removal experiment was conducted using the device shown in Fig. 3.1 (b). From the experimental results of the basic Sn removal characteristics in VHF plasma, the optimum conditions were a gas pressure of 35 Pa and a sample temperature of 20 °C, so these conditions were fixed. The power was 30 W. The plasma exposure time was set to 6 min so that the amount of Sn film removed did not exceed 50 nm in thickness. In order to investigate the dependence of Sn removal on the hydrogen

gas flow rate, the change in Sn film thickness was measured by changing the hydrogen gas flow rate to 20, 40, and 60 sccm. The results are shown in Table 3.1. As can be seen from the table, a peak etching rate of 8.3 nm/min was obtained with a hydrogen gas flow rate of 20 sccm. As a result of probe measurement under the cylinder provided in the center of the partition metal plate, an electron density of 6.6×10^{15} m^{-3} and an electron temperature of 3 eV were obtained. When the efficiency as RIE is evaluated based on these data, the Sn yield is 0.12. Taking the reciprocal, this corresponds to the removal of one Sn atom by 8.1 hydrogen ions. The efficiency of this Sn removal is lower than the above-mentioned maximum value when the VHF plasma alone is used.

As can be seen from Table 3.1, the results of this experiment incorporating the hollow cathode discharge clearly contradict the results of Fig. 3.7 in that the amount of Sn removed decreases with the hydrogen gas flow rate. This experimental result suggests that it is out of the optimum conditions. In this arrangement, the flow of hydrogen gas is orthogonal to the plasma ejected from the hollow cathode discharge, and the higher the hydrogen gas flow rate, the more likely it is that the irradiation of the plasma on the Sn sample surface is hindered. This means that, in the current equipment configuration, the relationship of Sn removal with respect to the hydrogen gas flow rate cannot be optimized, and it is necessary to improve the equipment in order to obtain the optimum etching rate.

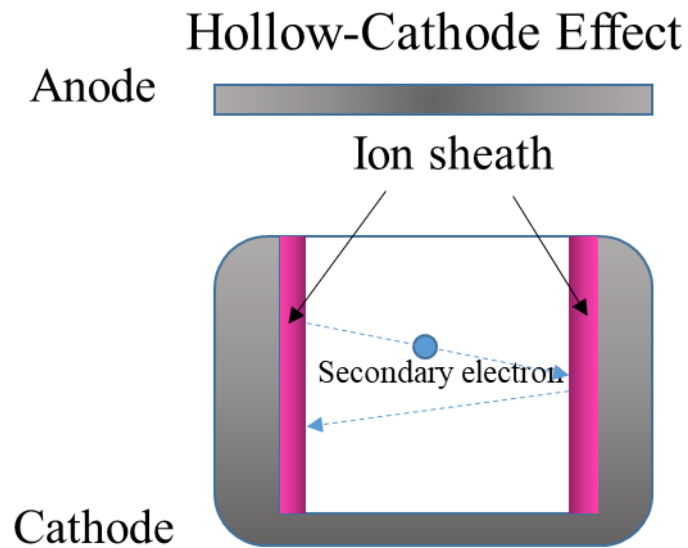

Fig. 3.9 Schematic of formation for hollow-cathode discharge.

Gas flow rate [sccm]	Thickness of decomposed Sn [nm]	Etching rate [nm/min]
20	49.7	8.3
40	48.8	8.1
60	34.7	5.8

Table 3.1 Results of Sn decomposition for hollow cathode discharge.

3.4 Conclusion

In this chapter, in order to clarify the possibility of efficient Sn debris removal by VHF hydrogen plasma, we first investigated the efficiency and characteristics of Sn removal with respect to hydrogen gas pressure, hydrogen gas flow rate, and Sn sample temperature. As a result, an etching rate of 4.8 nm/min was achieved. The following conclusions were obtained from these basic data. (i) The higher the electron density, the better to promote RIE and increase the etching rate. (ii) If the gas pressure is high and SnH_4 is not sufficiently separated from the Sn sample surface, readhesion is likely to occur. (iii) To prevent readhesion, it is effective to increase the gas flow rate and lower the Sn sample temperature. In order to increase electron density, hollow cathode discharge was combined with VHF discharge. As a result, the electron density was more than doubled, and the maximum etching rate of 8.3 nm/min was obtained. However, the Sn yield value for evaluating the efficiency of RIE was reduced to about 60% in the case of the VHF discharge alone.

In a device in which the hollow cathode effect is superimposed on the VHF discharge, the etching rate is expected to be further improved by optimizing the gas flow so as to promote the separation of SnH_4 from the Sn surface.

References

[1] News release by TSMC, Oct 7, 2019, https://www.tsmc.com/tsmcdotcom/PRListingNewsAction.do?action=detail&language=E&newsid=THHIHIPGTH

[2] H. Mizoguchi, H. Nakarai, T. Abe, K. M. Nowak, Y. Kawasuji, H. Tanaka, Y. Watanabe, T. Hori, T. Kodama, Y. Shiraishi, T. Yanagida, T. Yamada, T. Yamazaki, S. Okazaki, T. Saitou, Proc. SPIE, 1009702 (2017).

[3] H. Mizoguchi, H. Nakarai, T. Abe, T. Ohta, K. M. Nowak, Y. Kawasuji, H. Tanaka, Y. Watanabe, T. Hori, T. Kodama, Y. Shiraishi, T. Yanagida, T. Yamada, T. Yamazaki, S. Okazaki, T. Saitou, Proc. SPIE, 867986790A (2013).

[4] Gunther Nicolussi, Eugen Beck, IEEE SEMI Advanced Semiconductor Manufacturing Conference. 0-7803-71 (2002).

[5] H. Tanaka, A. Matsumoto, K. Akinaga, A. Takahashia, T. Okada, Appl. Phys. Lett. 87, 5 (2005).

[6] M.M.J.W. van Herpen, D.J.W. Klunder, W.A. Soer, R. Moors, V. Banine, Chem. Phys. Lett. 484, 197 (2010).

[7] D. Ugur, A. J. Storm, R. Verberk, J. C. Brouwer, W. G. Sloof, Chem. Phys. Lett. 552, 122 (2012).

[8] D. Ugur, A.J. Storma, R. Verberk, J.C. Brouwer, W.G. Sloof, Appl. Surf. Sci. 288, 673 (2014).

[9] D. T. Elg, J. R. Sporre, G. A. Panici, S. N. Srivastava, D. N. Ruzic, J. Vac. Sci. Technol. A, Vac. Surf. Film. 34, 021305 (2016).

[10] D. T. Elg, G. A. Panici, S. Liu, G. Girolami, S.N. Srivastava, D. N. Ruzic1, Plasma Chem. Plasma Process. 38, 223 (2018).

[11] M. Ji, R. Nagata, K. Uchino, Plasma Fusion Res. 16, 1406003 (2011).

[12] L. Birdos, Surface and Coatings Technology, 86-87, 648 (1996).

[13] Y.Ohtsu and Y.Kawasaki, J. Appl. Phys. 113, 033302 (2013).

[14] K. Tamaru, J. Phys. Chem. 60 (1956) 610.

[15] L. St-Onge and M. Moisan, Plasma Chem. Plasma Process. 14, 87 (1994).

[16] M. A. Lieberman and A. J. Lichtenberg, "Principles of Plasma Discharges and Materials Processing", 2nd ed., Wiley, Hoboken, NJ, (2005) p188.

Chapter 4 Effect of Hydrogen Ion Energy in the Process of Reactive Ion Etching of Sn Thin Films by Hydrogen Plasmas

4.1 Introduction

Extreme ultraviolet (EUV) lithography, employing a light wavelength of 13.5 nm, has been successfully applied in the mass production of semiconductors using 7-nm node processes [1]. EUV lithography uses emissions from multiply charged tin (Sn) ions, as generated by the laser irradiation of Sn droplets with diameters of approximately 20 μm. Currently available sources for EUV lithography systems are typically based on high-density hot Sn plasmas [2,3]. Sn droplets bombarded by lasers produce Sn debris adhering to the surface of the collection mirror, resulting in the deterioration of the reflectance. Therefore, it is necessary to efficiently decompose the Sn debris adhered to the mirror surface.

Studies have proposed etching the Sn debris through a chemical reaction between a Sn atom and four hydrogen atomic radicals, thereby producing the volatile molecule SnH_4 [4,5]. Ugur [5] produced hydrogen atoms using a hot filament method, and introduced them to the surface of Sn thin films. The decrease in the thin films was quantitatively measured, and it was found that approximately 90 000 hydrogen atoms were necessary to produce one SnH_4 molecule [5]. In a real EUV system, EUV photons (energy 92 eV) dissociate hydrogen gas, which fills the EUV source chamber at approximately 10 Pa; the generated SnH_4 molecules from the Sn etching are evacuated from the chamber, together with the hydrogen gas. Elg et al. [6] proposed an additional Sn removal system based on using an EUV mirror as a powered electrode, and produced a hydrogen plasma using a radio frequency power source at a frequency of 13.56 MHz. The plasma could directly supply hydrogen atoms to the surface of the EUV mirror. Subsequently, Elg et al. also claimed [7] that reactive ion etching, which utilizes hydrogen ion energy, can more efficiently remove Sn films adhered on an EUV mirror surface than etching using hydrogen atoms alone. In their experimental device, a self-bias voltage of approximately -300 V appeared at the powered electrode simulating the EUV mirror, and the average hydrogen energy was

estimated to be more than 300 eV [6].

Reactive ion etching has already been investigated as a method for removing carbon (C) thin films deposited on an EUV mirror surface [8–10]. The method utilizes the synergistic effects between hydrogen atoms and argon or hydrogen ions to etch C and generate CH_4 (or other volatile hydro-carbon molecules).

In this C etching, the bond energy of the C is approximately 7 eV, and it has been found that the etching progresses as the ion energy increases [8,10]. In contrast, the bond energy of Sn is as low as approximately 3 eV (as described later); therefore, the hydrogen ion energy dependence of the Sn etching is considered as different from that of the C etching. The authors obtained a much higher Sn etched thickness per minute than those obtained by Elg et al. [7]. We used a very VHF (high-frequency) hydrogen plasma, and samples with Sn thin films (hereafter referred to as "Sn samples") were set on a grounded electrode [11]. The hydrogen ions impinging on the Sn sample through the ion sheath should have had energies of approximately 10 eV.

Based on the above, we investigated the dependence of the hydrogen energy on the Sn etching. We applied various bias voltages to Sn samples, and arranged the plasma so as to be at a stable space potential, so that we could examine the threshold hydrogen ion energy for Sn etching (currently thought to be a few eV).

4.2 Experimental setup and methods

The Sn samples were Si substrates with an area of 15 × 15 mm^2 and thickness of 0.625 mm. The samples were covered by deposited Sn thin films, each with a thickness of approximately 100 nm. The etched thicknesses of the Sn thin films were quantitatively measured via X-ray fluorescence (XRF) analysis. The details of the analysis will be described later.

A schematic diagram of the experimental device is shown in Fig. 4.1(a). The vacuum chamber was divided into upper and lower spaces by a metal partitioning plate with a thickness of 3 mm. The side wall of the upper space was a quartz glass tube with an inner diameter of 62 mm. The upper surface of

the upper space was the powered electrode, and the spacing between the powered electrode and partitioning plate at the ground potential was approximately 30 mm. A VHF power source at a frequency of 60 MHz supplied a power of 15 W to the powered electrode, and the hydrogen plasmas were produced in the upper space.

The lower space was formed in a stainless-steel block with an outer radius of 112 mm. The lower space had a radius of 56 mm and cutting depth of 16 mm. The ceiling of this space comprised the partitioning metal plate. As the stainless-steel block was grounded, the lower space was surrounded by a circular side wall at the ground voltage. At the bottom of this lower space, a structure was installed to apply DC bias voltages to the Sn samples. The height of the surface of the Sn sample was 3 mm from the bottom. The electron density and electron temperature were measured using a Langmuir probe at 4 mm above the Sn surface (7 mm above the bottom surface). The measuring part of the probe comprised cylindrical tungsten with a length of 10 mm and diameter of 0.5 mm. The probe was inserted through a port hole provided on the side wall with a diameter of 6 mm (the center height was 7 mm from the bottom). There were three other holes with the same diameter, which were used for gas pressure monitoring, H_2 gas introduction, and lead wire introduction for the DC bias voltage. At the outside of the vacuum chamber, a small resistor was inserted into the lead wire circuit, and the voltage across the resistor was measured to determine the current flowing into the Sn sample. In addition, the voltage on the sample side was measured. A port hole with a diameter of 12 mm was also provided on the side wall, through which the vacuum chamber was evacuated.

A hole with a diameter of 26 mm was made in the center of the partitioning metal plate, and two metal meshes were attached to both the upper and lower surfaces of the partitioning metal plate. The VHF hydrogen plasma generated in the upper space passed through these meshes by diffusion, and by the gas flow owing to the evacuation from the lower space. The Sn sample was exposed to the hydrogen plasma that entered the lower space in this way. As described above, the lower space was surrounded by the metal of the grounded potential, and therefore, the fluctuation of the space potential of the plasma in the lower space was much smaller than that of the plasma in the upper space, where the potential

fluctuation was large. As a result, the potential of a Sn sample surface potentially floated with respect to the chamber could be determined using the bias voltage. In fact, fluctuations of approximately ±0.1 V appeared in the floating voltages of the Sn samples. Simultaneously, the mesh spacing (1.55 mm) and wire diameter (0.2 mm) were adjusted to secure the electron density in the middle of 10^{15} m^{-3}, so that sufficient Sn etching would occur.

Over 20 holes (each with a diameter of approximately 3 mm) were made around the hole with the diameter of 26 mm on the partitioning metal plate. We intended to supply the hydrogen gas supplied to the lower space to the upper space as well, i.e., through the hole with a diameter of 26 mm and these small holes. Under a gas pressure of 30 Pa, no hollow cathode discharge occurred in these small holes, i.e., there was no plasma supply to the lower space through these holes.

As shown in Fig. 4.1(b), the lower space was provided with a structure for applying a bias voltage to the Sn sample. From the bottom of the lower space, the following elements were layered in order: a metal base plate (thickness 1 mm), mica plate (thickness 0.2 mm) for insulation, metal substrate holder surrounded by a Teflon spacer (both thicknesses 1.5 mm), Sn substrate (0.62 mm buried in the substrate holder and approximately 0.12 mm above the substrate holder surface), press metal plate (thickness 0.1 mm) at the bias voltage, Teflon spacer (thickness 0.3 mm), and grounded metal plate (thickness 0.1 mm). These elements were then fixed with screw rods and nuts at the four corners. A 12×12 mm^2 area square hole was drilled in the center of the press metal plate, Teflon spacer, and grounded metal plate. As described above, the sample holder was connected to a DC power supply, so that a bias voltage could be applied from the outside.

After evacuating the vacuum vessel to 4×10^{-2} Pa, hydrogen gas was flowed at a rate of 40 sccm using a mass flow controller, and was adjusted with a butterfly valve to maintain the pressure at 30 Pa. All measurements in this study were performed at this gas pressure.

For some Sn samples, the actual film thickness was measured by the crystal oscillator method; these were used as calibration samples. As the thickness of the Sn film (target value 100 nm) varied by ±10%, the Sn Lα signal of the XRF was calibrated using the calibration samples. First, the film thicknesses of

the Sn samples were measured before exposure to the hydrogen plasma. Then, the film thicknesses were measured again after the experiment, to quantify the amount of Sn removed by the plasma exposure.

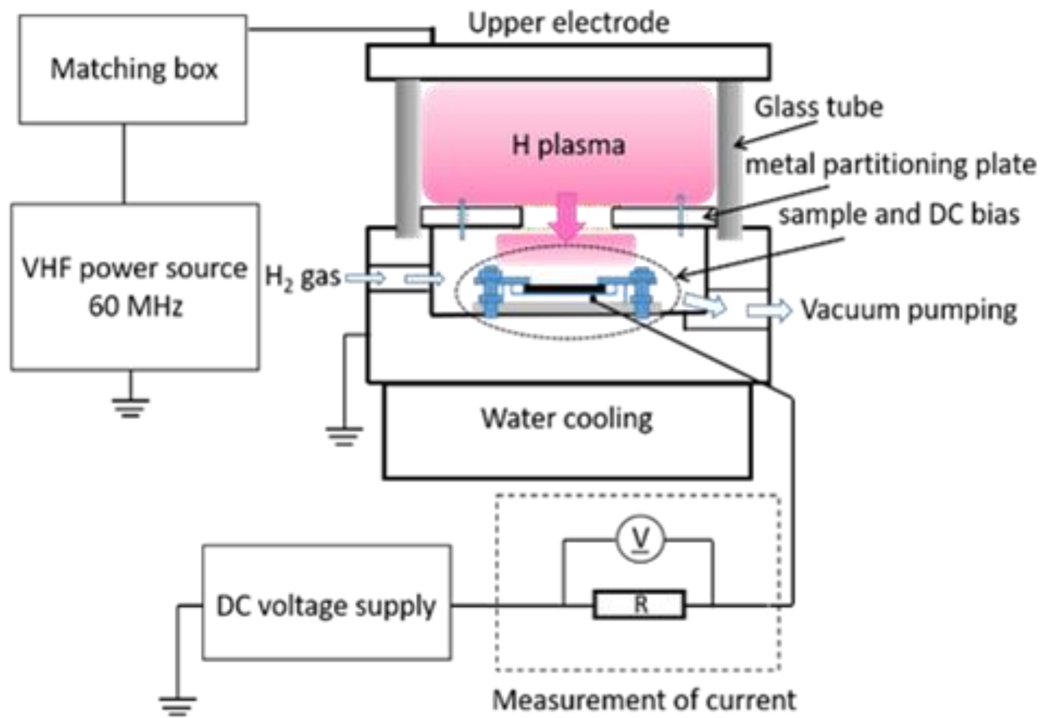

(a)

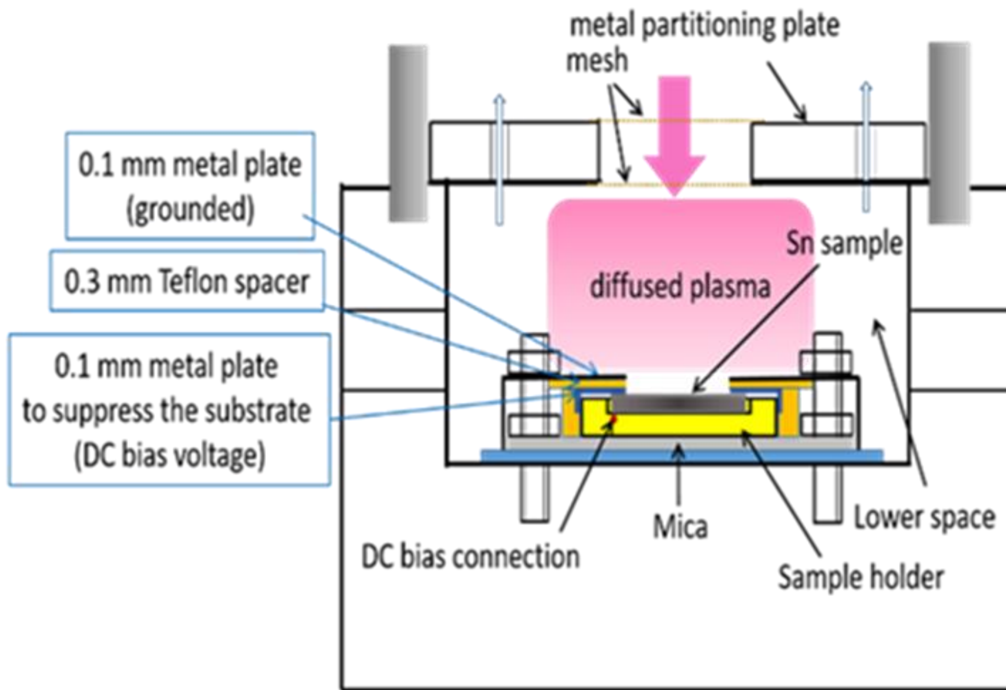

(b)

Fig. 4.1 (a) Schematic of the experimental setup. (b) Schematic of the side view of the DC bias structure.

4.3 Experimental results and discussion

As described in Section 2, the electron density and electron temperature above the Sn sample were measured using a Langmuir probe, and an example of the current-voltage characteristic curve is shown in Fig. 4.2. The electron temperature was evaluated as $T_e = 2.8$ eV from a logarithmic plot of the electron current with respect to the voltage. From the ion saturation current at the floating voltage, the electron density was evaluated as $n_e = 5 \times 10^{15}$ m^{-3}. The floating voltage of the Sn sample was $V_f = 3.2$ V.

Under the experimental conditions of this study, most of the hydrogen ions were H_3^+ when calculated according to Reference [12], so it was assumed that all hydrogen ions were H_3^+. The measured value of the plasma potential V_p was 7.5 V when evaluated from the current-voltage characteristics using an Sn sample. As the electrons of the diffused plasma were collected by using the 12-mm square Sn sample as a probe, it is highly possible that the plasma was disturbed. According to probe theory, the difference between V_p and V_f can be expressed as follows [13]:

$$\left|V_p - V_f\right| = \frac{T_e}{2} \times \ln\left(1 + \frac{m_i}{2\pi m_e}\right) \tag{4.1}$$

where m_i is the mass of the hydrogen ion (3 amu), and m_e is the mass of the electron. From this, we can evaluate $|V_p - V_f| = 10.9$ V; in the following, we consider $V_p = 14.1$ V.

The DC bias voltage V_b was varied at 7.5, 5, 0, -10, -30, and -50 V, and was applied to the Sn samples. The Sn samples were exposed to hydrogen plasma for 15 min, and the Sn etched thicknesses were examined. The results are shown in Fig. 4.3. The error bars in the figure illustrate the standard deviations from the results of five to six measurements at each bias voltage.

The current flowing into the Sn sample at each DC bias was also measured. The results are shown in Fig. 4.4. This result is basically a current-voltage characteristic curve of the saturated ion current, based on using the Sn sample as a planar probe. On the negative side of the DC bias voltage of -10 V, there is no influence of the electron current, i.e., it is purely ion current. Because the measurement points for the DC bias voltages -10, -20, and -30 V are on one straight line, the fitted line (shown in Fig. 4.4 by a red line) was extended to 3.2 V (floating voltage) to estimate the ion currents, as in the probe analysis.

Table 4.1 shows the value of the ion current obtained in this way as an underlined value with respect to the DC bias voltage. Table 4.1 also shows the thickness of the ion sheath d_s. The following equation was used for this calculation [13]:

$$d_s = 0.47 \times \lambda_D \sqrt[\frac{3}{2}]{\frac{2V_0}{T_e}} \quad (4.2)$$

where λ_D is the Debye length, and V_0 is the voltage applied to the ion sheath (= $V_s - V_b$).

As mentioned in Section 2, the plasma exposure area of the Sn sample is limited to 12 × 12 mm^2 by the grounded metal plate. The Sn sample surface is 0.5 mm lower than the metal plate surface. At a floating voltage of 3.2 V, the sheath thickness d_s = 0.39 mm; therefore, the area of the ion sheath can be considered as 12 × 12 mm^2. The ion current is estimated as a product of the Bohm flux, elementary charge, and surface area of the sheath. The ion current value obtained in this way is 0.66 mA, which is in good agreement with the ion current value of 0.74 mA at a floating voltage of 3.2 V (Table 4.1). The situations are the same for V_b = 5 and 7.5 V; therefore, both ion current values are considered as 0.74 mA, as shown in Table 4.1.

The last row of Table 4.1 shows the Sn atom yield which is the number of Sn atoms removed per hydrogen ion, and this value is considered to indicate the efficiency of the reactive ion etching. The values of the Sn yield are obtained from the total amount of removed Sn atoms as evaluated from Fig. 4.3, divided by the total amount of hydrogen ions after 15 min of plasma exposure. At a bias voltage of 0 V, the Sn yield has the maximum value, meaning that one Sn atom is removed per (approximately) 70 hydrogen ions.

The Sn etched thickness using hydrogen atoms alone was investigated, under the condition that the influence of the hydrogen ions was almost eliminated. Specifically, a grounded metal mesh was placed approximately 2 mm above the grounded metal plate, and a +7.5 V bias was applied to the Sn sample. As a result, the Sn etched thickness (removed after 15 min of plasma exposure) was 1.2 nm on average for the four measurements. Considering the reported fact [5] that 9×10^4 hydrogen atoms are necessary to remove one Sn atom, the hydrogen atom density can be evaluated as 8×10^{18} m^{-3} (dissociation degree

of approximately 0.1%) from this etched thickness. It can be seen from Fig. 4.3 that the Sn etched thicknesses for bias voltages below 5 V are more than 10 nm. Therefore, it was confirmed that etching involving hydrogen ions is at least an order of magnitude more dominant than that using atoms alone.

We also can consider the binding energy of Sn in a metal bond. The standard sublimation enthalpy of metallic β phase tin is 302.1 kJ/mol, and the tin metal has a body-centered cubic structure with four bonds between atoms. The binding energy per Sn atom can be obtained from the standard sublimation enthalpy [8]; as calculated in eV units, the value is 3.1 eV, i.e., 0.78 eV per bond.

As mentioned in the introduction, reactive ion etching has been examined for the removal of C films deposited on an EUV mirror [8–10], and Hoph's model [8] has been proposed as the mechanism. According to the model, when the bond between carbons (bonding energy 7.4 eV) is broken by the energy of the ions, a bond between the carbon and hydrogen is formed by the flux of the hydrogen atoms, which is more than two orders of magnitude higher than the ion flux. From this chemical reaction, volatile and stable hydrocarbon molecules (CH_4, etc.) are generated. In the experiments of Hoph et al. [8], argon ion energies in the range of 20–800 eV were investigated, and it was found that the erosion yield of the carbon increased monotonically with the argon ion energy. Sputtering occurs depending on the energy of argon ions, and even if hydrocarbon molecules are formed relatively deep from the surface, the stable hydrocarbon molecules diffuse to the surface, and are discharged into the gas phase. Such a process has been examined theoretically [10], and comparisons with experimental results have shown the usefulness of this model. Similar results were obtained by Dolgov et al. [9] using hydrogen plasma (hydrogen ion energies 20–100 eV).

In contrast, the Sn decomposition is not a monotonically increasing function of the hydrogen ion energy, as shown in the last row of Table 4.1. A bias voltage of +7.5 V (hydrogen ion energy of approximately 7 eV) is the threshold for Sn etching, and the Sn yield becomes maximum between a bias voltage of 0 V and floating voltage of 3.2 V (hydrogen ion energy of approximately 10–14 eV). At higher hydrogen ion energies, the Sn yield drops, or remains at a nearly constant value. One reason for the hydrogen ion-energy dependence of the Sn yield is that the difference in mass between an H_3^+ ion and Sn atom is large.

When considered as a simple head-on collision between rigid spheres, the energy that H_3^+ ions (mass 3 amu) can give to Sn atoms (mass approximately 119 amu) is approximately four times the mass ratio, i.e., approximately 10% of the ion energy. Moreover, 10% of the threshold energy of the Sn decomposition is equal to the energy of one Sn metal bond. Another reason could be that SnH_4 is an unstable molecule. It has been shown by Tamaru [14] that the activation energy for the dissociation of SnH_4 on a Sn surface is approximately 0.4 eV per molecule. Therefore, the exothermic reaction of $SnH_4 \rightarrow Sn + 2H_2$ spontaneously proceeds, even at room temperature. Furthermore, as SnH_4 is 10 times heavier than CH_4, it is difficult for SnH_4 to escape via diffusion from the inside of the Sn film to the surface. The reactive ion etching for Sn decomposition is considered to occur only at a very shallow position from the surface of the Sn film. When a penetration depth of the H_3^+ ions into the Sn film is calculated using the "Stopping and Range of Ions in Matter" code [15], most of the ions penetrate to a depth of 2 nm or more from the film surface, at an ion energy of 30 eV or higher. The contribution of these ions to the Sn decomposition may be small.

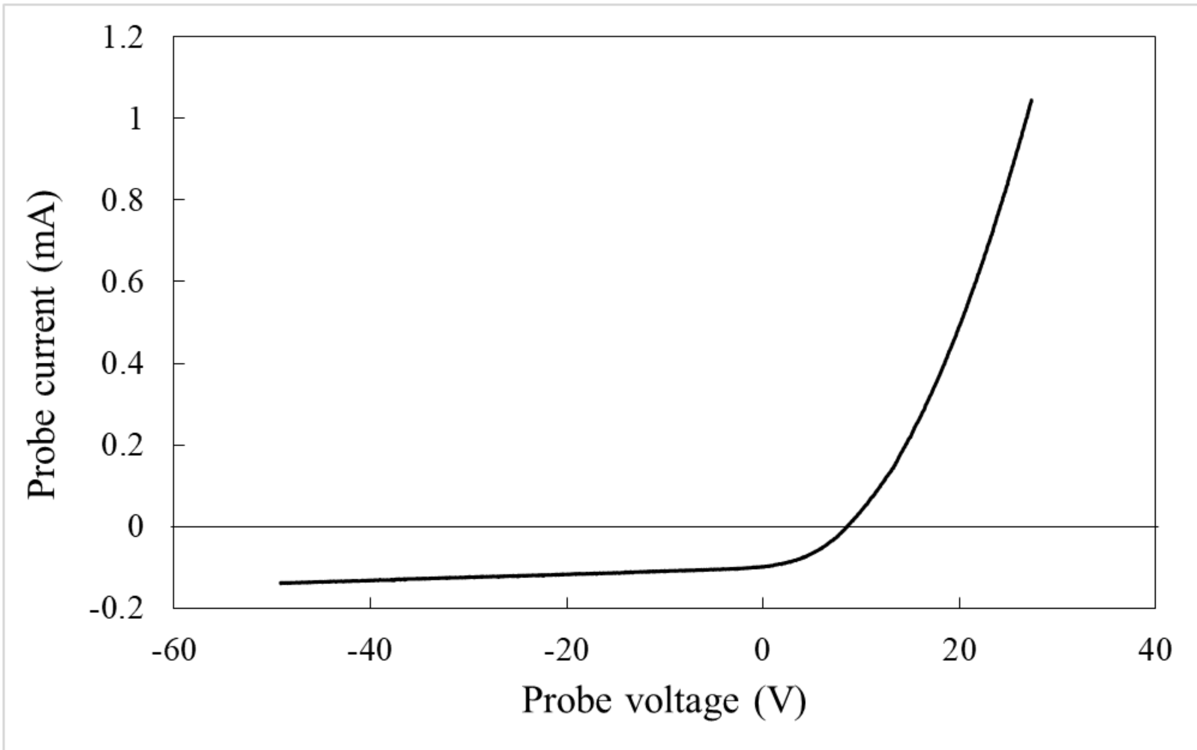

Fig. 4.2 Probe characteristic *I-V* curve.

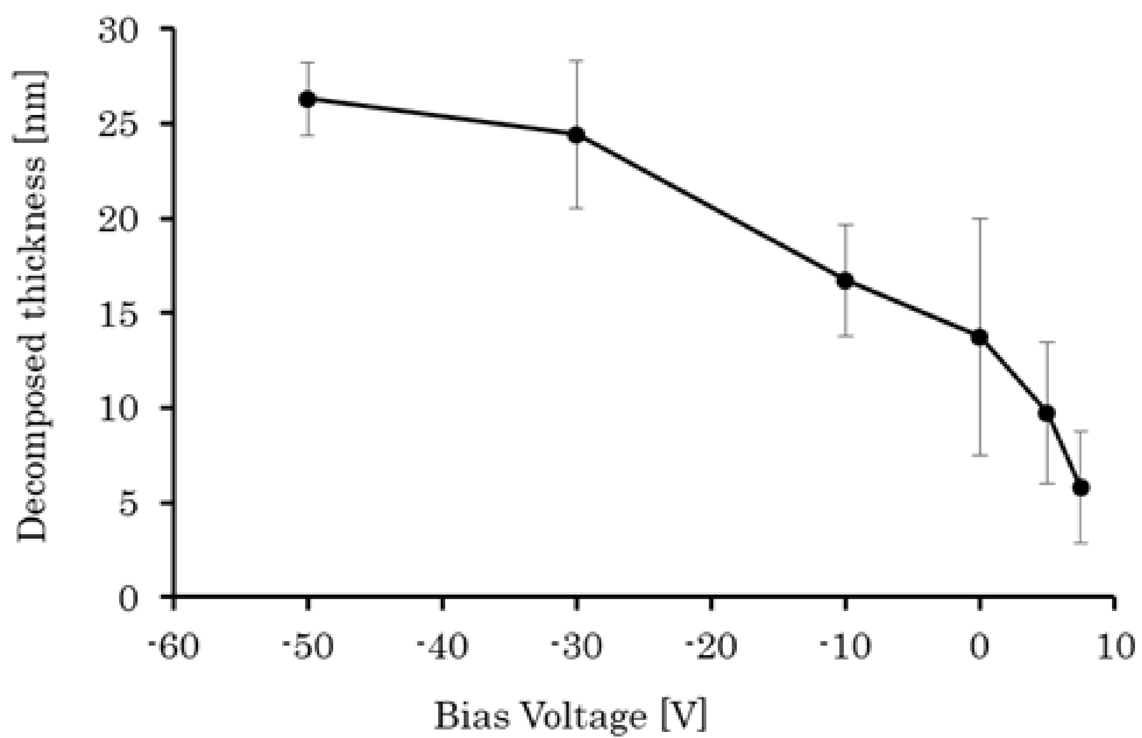

Fig. 4.3 Decomposed thickness of Sn film after plasma exposure of 15 minutes as a function of the DC bias voltage.

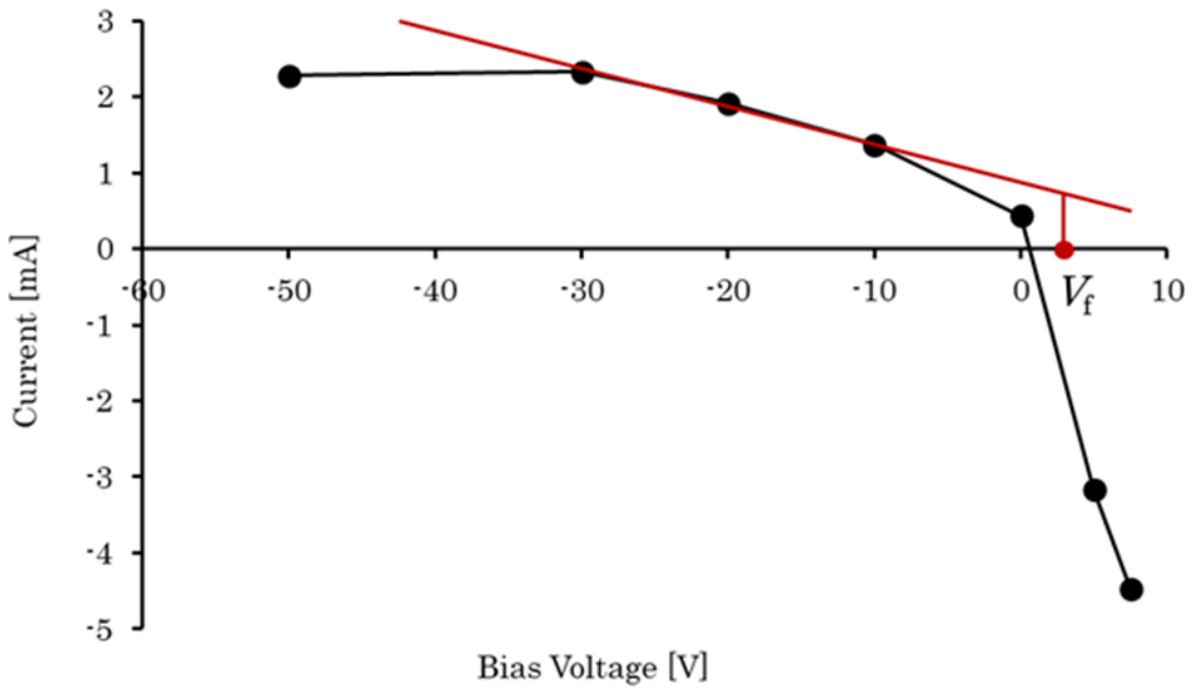

Fig. 4.4 Current flowing into Sn sample during plasma exposure as a function of the DC bias voltage.

Bias voltage (V)	7.5	5	3.2	0	-10	-30	-50
Sheath voltage (V)	6.6	9.1	10.9	14.1	24.1	44.1	64.1
Ion current (mA)	<u>0.74</u>	<u>0.74</u>	<u>0.74</u>	0.89	1.37	2.33	2.28
Thickness of ion sheath (mm)	0.26	0.34	0.39	0.47	0.70	1.10	1.46
Sn yield ($\times 10^{-2}$ atoms/ion)	0.75	1.25	—	1.47	1.16	1.00	1.10

Table 4.1 Values to evaluate Sn etching efficiency for each DC bias voltage. The last row shows the resultant efficiency as the number of removed Sn atoms per one hydrogen ion.

4.4 Conclusion

In this study, we investigated the ion energy dependence of Sn reactive ion etching by hydrogen atoms and ions. The Sn atom yield per hydrogen ion did not increase with the ion energy (contrary to the results reported for C-film etching) and became constant or decreased with hydrogen ion energies of approximately 30 eV or more. The threshold ion energy for Sn etching was 10 eV or less, and the peak of the Sn yield appeared when the ion energy was approximately 10–14 eV. This means that it is efficient to use the floating voltage in hydrogen plasma when removing the Sn film adhered to an EUV mirror, which is electrically insulating. This result is quite favorable for the actual decomposition of Sn debris films from EUV mirrors.

References

[1] *News* release by TSMC, Oct 7, 2019, https://www.tsmc.com/tsmcdotcom/PRListingNewsAction.do?action=detail&language=E&newsid=THHIHIPGTH

[2] H. Mizoguchi, H. Nakarai, T. Abe, T. Ohta, K. M. Nowak, Y. Kawasuji, H. Tanaka, Y. Watanabe, T. Hori, T. Kodama, Y. Shiraishi, T. Yanagida, T. Yamada, T. Yamazaki, S. Okazaki, T. Saitou, Proc. SPIE, 867986790A (2013).

[3] H. Tanaka, *et al*., Appl. Phys. Lett. 87, 5 (2005).

[4] M.M.J.W. van Herpen, D.J.W. Klunder, W.A. Soer, R. Moors, V. Banine, Chem. Phys. Lett. 484, 197 (2010).

[5] D. Ugur, A. J. Storm, R. Verberk, J. C. Brouwer, W. G. Sloof, Chem. Phys. Lett. 552, 122 (2012).

[6] D. T. Elg, J. R. Sporre, G. A. Panici, S. N. Srivastava, D. N. Ruzic, J. Vac. Sci. Technol. A, Vac. Surf. Film. 34, 021305 (2016).

[7] D. T. Elg, G. A. Panici, S. Liu, G. Girolami, S.N. Srivastava, D. N. Ruzic1, Plasma Chem. Plasma Process. 38, 223 (2018).

[8] C. Hopf, A. von Keudell, W. Jacob, J. Appl. Phys. 94, 2373 (2003).

[9] A. Dolgov, D. Lopaev, T. Rachimova, A. Kovalev, A. Vasil'eva, C. J. Lee1, V. M. Krivtsun, O. Yakushev and F. Bijkerk, J. Phys. D Appl. Phys. 47, 65205 (2014).

[10] S. Liu, J. Sun, S. Dai, T. Stirner, D. Wang, J. Appl. Phys. 108, 073302 (2010).

[11] M. Ji, R. Nagata, K. Uchino, Engineering Sciences Report, Kyushu University, 42-2, 12 (2021).

[12] L. St-Onge and M. Moisan, Plasma Chem. Plasma Process. 14, 87 (1994).

[13] M. A. Lieberman and A. J. Lichtenberg, "Principles of Plasma Discharges and Materials Processing", 2nd ed., Wiley, Hoboken, NJ, (2005) p188.

[14] K. Tamaru, J. Phys. Chem. 60, 610 (1956).

[15] J.F. Ziegler et al., Nuclear Instruments and Methods in Physics Research B **268**, 1818 (2010).

Chapter 5 Conclusion

5.1 Summary of this study

In this study, we have examined Sn decomposition using VHF hydrogen plasmas (at a frequency of 60MHz). The VHF plasmas were produced in a compact reactor and Sn decomposition experiments were performed. In the experiments, the dependences of Sn decomposition on hydrogen gas pressure, gas flow rate and sample temperature were investigated. In addition, we added DC bias section to the bottom of the chamber, which is floated from the ground potential. Then, DC bias voltages were applied in the range from -50V to 7.5V to the Sn sample surface covered by the Sn thin film. Using this system, the role of ion hydrogen energy in the process of reactive ion etching.

The characteristics of the VHF plasmas were clarified based on the measurements using Langmuir probe method. SEM observation and X-ray fluoresce analysis are employed as measurement techniques to evaluate the surface variation and perform quantitative analysis, respectively.

The achievements of this study are summarized as below:

1. From the basic experiments investigating the dependences of Sn decomposition on hydrogen gas pressure, gas flow rate and sample temperature, following conclusions were drawn. (i) The higher the electron density, the more reactive ion etching can be promoted and the etching rate can be increased. (ii) If the gas pressure is high and SnH_4 is not sufficiently separated from the Sn sample surface, re-adhesion may occur. (iii) It is effective to increase the gas flow rate and lower the Sn sample temperature to prevent re-adhesion.
2. The peak etching rate in the basic experiments was 4.8 nm/min and this was obtained at the gas pressure of 35 Pa. This etching rate gives us the number of Sn atoms removed in one

minute. Also, the total number of hydrogen ions impinged on the surface of the Sn thin film in one minute were estimated because the values of electron density and electron temperature were measured. Based on these estimates, Sn yield (the number of tin atoms removed per hydrogen ion: Sn atoms/ion) was calculated as the etching efficiency of Sn removal with respect to hydrogen ions. The result gave the Sn yield value of 0.20 and showed effectiveness of the ion reactive etching in the process of Sn removal.

3. Hollow cathode discharge was combined with VHF discharge to increase the etching rate. As a result, the electron density was more than doubled, and a maximum etching rate of 8.3 nm/min was obtained. However, the Sn yield value was reduced to about 60% for the case that the VHF discharge was used alone. From the opposite point of view, it is suggested that the Sn etching rate by the VHF plasma when combined with the hollow cathode discharge can be further improved if the gas flow conditions are optimized.
4. The ion energy dependence of Sn reactive ion etching by hydrogen atoms and ions were investigated. The results showed that the Sn atom yield per hydrogen ion did not increase with the ion energy and became constant or decreased with hydrogen ion energies of approximately 30 eV or more. The threshold ion energy for Sn etching was 10 eV or less, and the peak of the Sn yield appeared when the ion energy was approximately 10–14 eV. This means that it is efficient to use the floating voltage in hydrogen plasma when removing the Sn film adhered to an EUV mirror, which is electrically insulating. This result is quite favorable for the actual decomposition of Sn debris films from EUV mirrors.

5.2 Suggestion for the future work

We tried to obtain much higher Sn etching rate by using the hollow cathode discharge. However, the result was not we expected. In that experiment, the flow of hydrogen gas was

orthogonal to the plasma diffused from the hollow cathode discharge, and the higher the hydrogen gas flow rate, the more likely it is that the irradiation of the plasma on the Sn sample surface is hindered. This means that the hydrogen gas flow must be optimized to obtain the maximum etching rate.

Acknowledgement

It was my fortune that I had a chance to study in Uchino laboratory 5 years ago. How time flies. My study at Kyushu University will soon come to an end. At the completion of my doctoral thesis, I wish to express my gratitude to the people who helped me so much.

First and foremost, I would like to give a sincere gratitude to my supervisor Prof. Uchino Kiichiro for his guidance, support, encouragement, and patience throughout my study at Kyushu University. During the past 5 years, his great ideas and wide knowledge helped me overcome many problems in my research. His intelligence in research study really inspires me a lot. In particular, his creative ideas and enthusiastic attitude in scientific research gives me deep impression. It is my honor to be his student. I believe these invaluable experience will benefit all my life. I must thank Prof. Hattori Reiji and Prof. Hayashi Nobuya for reviewing my thesis work and their comments. Appreciate to Prof. Kawai Yoshinobu for his valuable advices in the experiments.

I would like to give thanks to other members in Uchino laboratory. Thank Prof. Yamagata Yuihiko and Prof. Tomita Kentaro for their valuable advices in study and research. Appreciate to Mrs. Sakurai for her kind helping in campus life. Furthermore, to the members in our group Mr. Nagata Ryo, Mr. Imada Rei and Mr. Sato Shusuke, appreciate to the help in experiment and research.

Moreover a cordial gratitude goes to my family and friends who is supporting me all these years during my study.